

**Study Of Nickel Copper Ferrite Nanoparticles
Synthesised Using Combustion Method**

A dissertation for PHY-651

Credits: 16

Submitted in partial fulfillment of Masters Degree

M.Sc. in Physics

by

ROHIT SUKDO FADTE

Roll Number: 22P0430031

ABC ID: 993-614-730-086

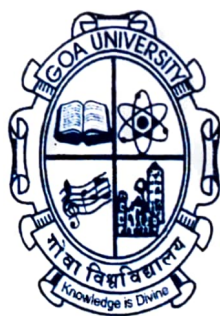
PRN: 201905817

Under the supervision of

Dr. Pranav. Naik

School Of Physical and Applied Science

Physics Discipline



Goa University

May 2024



Examined by:

R. S. Fadte

Seal of the School

DECLARATION BY STUDENT

I hereby declare that the data presented in this Dissertation report entitled, "Study of Nickel Copper Ferrite Nanoparticles Synthesised using Combustion Method" is based on the results of investigations carried out by me in the Physics Discipline at the School of Physical and Applied Sciences, Goa University under the Supervision of Dr. Pranav P. Naik. and the same has not been submitted elsewhere for the award of a degree or diploma by me. Further, I understand that Goa University or its authorities will be not be responsible for the correctness of observations / experimental or other findings given the dissertation.

I hereby authorize the University authorities to upload this dissertation on the dissertation repository or anywhere else as the UGC regulations demand and make it available to any one as needed.



Name: Mr. Rohit .S. Fadte

Roll no:22PO430031

Date: 08/05/2024

Place: Goa University

COMPLETION CERTIFICATE

This is to certify that the dissertation report "Study of Nickel Copper Ferrite Nanoparticles synthesised using combustion method" is a bonafide work carried out by Mr. Rohit .S. Fadte under my supervision in partial fulfilment of the requirements for the award of the degree of M.Sc. in Physics at the School of Physical and Applied Sciences, Goa University.



Signature and name of Supervising Teacher: Dr. Pranav P. Naik

Date: 8/5/2024



Dean: Prof. Dr. Ramesh. Pai.

Date: 8/3/2024

Place: Goa University



ACKNOWLEDGEMENT

I am pleased to present the report of my project work undertaken during my final year in M.Sc. Physics. Although I have worked hard for the success of this project, it would not have been possible without the help and guidance of some people. Therefore, I would like to express my deep gratitude to those individuals.

Firstly, I would like to thank my project guide, Dr. Pranav P. Naik, for his excellent guidance, encouragement, intelligence and invaluable insight throughout the project. Thank you, Sir, for always motivating and inspiring me. Secondly, I would like to thank Ms. Sugania Chandavelou for her constant help and support throughout the project. Also, I would like to express my heartfelt gratitude towards the faculty members of the Department of Physics (SPAS) at Goa University for their continuous support and for creating a stimulating learning environment. I would like to thank the School of Physics and Applied Sciences for providing me with all the required instruments for my project work.

Next, I want to acknowledge all the PhD students in the Physics department who have assisted me by explaining how to use different instruments and software. I am also grateful to my family and friends for their unwavering support and encouragement throughout my studies.

Contents

Acknowledgement.....	i
List of figures.....	iv
Abstract.....	vi
❖ Chapter 1 – Introduction	
1 Nanomaterials.....	1
1.1 What are nanomaterials?.....	1
1.2 Classification of Nanomaterials.....	2
1.3 Why so much interest in nanomaterials?.....	3
1.4 Properties of Nanomaterials	4
1.4.1 Optical properties.....	4
1.4.2 Electrical Properties.....	5
1.5 Application of nanomaterials.....	5
2. Ferrites.....	6
2.1 Classification based on magnetic properties.....	7
2.2 Classification based on crystal structure.....	8
2.2.1 Normal Spinel Ferrite.....	9
2.2.2 Inverse Spinel Ferrite.....	9
2.3 Properties.....	10
References.....	11
❖ Chapter 2 – Literature Review.....	12
References.....	17
❖ Chapter 3 – Methods of Preparation	
3.1 Methods available for Ferrite nanopowder preparation.....	18
3.1.1 Co-precipitation Method.....	18
3.1.2 Auto-Combustion Method.....	19
3.1.3 Hydrothermal Method.....	20
3.2 Methods available for Thin Films preparation.....	21

3.2.1 Chemical deposition.....	21
a) Spin Coating.....	21
b) Spray pyrolysis.....	22
3.2.2 Physical deposition.....	23
a) Sputtering Method.....	23
b) Pulsed laser Deposition (PLD).....	25
3.3 Nickel copper ferrites by Auto-combustion method.....	26
References.....	28

❖ Chapter 4 - Characterisation Techniques

4.1 X-Ray diffraction.....	30
4.2 Scanning Electron Microscopy.....	31
4.3 UV-Vis spectroscopy.....	32
4.4 Raman spectroscopy.....	33
4.5 Electrical Measurements.....	35
4.6 Atomic Force Microscopy.....	38
References.....	40

❖ Chapter 5 – Results and Analysis

5.1 X-Ray diffraction.....	41
5.2 Scanning Electron Microscopy.....	46
5.3 Raman spectroscopy.....	48
5.4 Electrical Measurements.....	51
References.....	56

❖ Chapter 6 – Conclusion.....58

List of figures

<i>Figure 1 : Classification of Nanomaterials a) 0D spheres and clusters b) 1D nanowires, nanofibers and nanorods c) 2D nanofilms, nanoplates and networks d) 3D nanomaterials.....</i>	<i>3</i>
<i>Figure 2 : B-H curve of soft ferrites [3]</i>	<i>7</i>
<i>Figure 3 : B-H curve of Hard ferrites. [3]</i>	<i>8</i>
<i>Figure 4: The spinel structure of ferrites indicating the tetrahedral and octahedral sites. The divalent All cations occupy 1/8th of the tetrahedral voids, whereas the trivalent BIII cations occupy one half (1/2) of octahedral voids[5].</i>	<i>8</i>
<i>Figure 5: Structure of magnetic spinel ferrite showing tetrahedral sites (yellow), octahedral sites (green), and oxygen atoms (red) units (a) Unit cell structure of (b) normal spinel ferrite, and (c) inverse spinel ferrite.[4].....</i>	<i>9</i>
<i>Figure 6: schematic diagram of processes involved in co-precipitation method[1].....</i>	<i>19</i>
<i>Figure 7: Flow chart of processes involved in auto combustion[2].</i>	<i>20</i>
<i>Figure 8: The flowchart for synthesis of ferrite via hydrothermal method.[6].....</i>	<i>21</i>
<i>Figure 9: Spin coating various stages.[7]</i>	<i>23</i>
<i>Figure 10: Schematic diagram of Spray Pyrolysis Method.[9]</i>	<i>24</i>
<i>Figure 11: Schematic diagram of Sputtering.[8].....</i>	<i>24</i>
<i>Figure 12:Schematic diagram of RF Sputtering.[10]</i>	<i>25</i>
<i>Figure 13:Schematic diagram of Pulsed Laser deposition technique.[11]</i>	<i>26</i>
<i>Figure 14: Step by step process of making Ni Cu nanopowder by auto-combustion technique.....</i>	<i>28</i>
<i>Figure 15: Schematic diagram of X-Ray Diffraction Spectroscopy. [1,2].....</i>	<i>31</i>
<i>Figure 16: Rigaku Smart Lab X-Ray Diffractometer.</i>	<i>32</i>
<i>Figure 17: Schematic of a scanning electron microscope.[3].....</i>	<i>33</i>
<i>Figure 18: Schematic diagram of UV-Vis Spectrometer.[6].....</i>	<i>34</i>
<i>Figure 19: working of Raman spectroscopy.[10].....</i>	<i>35</i>
<i>Figure 20: Block Diagram of Electrical Network Analyser.....</i>	<i>38</i>

Figure 21: Electrical network analyser setup.	39
Figure 22: Schematic Diagram of Atomic Force Microscopy.[13]	40
Figure 23: Rigaku Smart-Lab X-ray Diffractometer	42
Figure 24 : Reitveld refined XRD patterns of Nickel Copper ferrite nanopowder.	45
Figure 25 : (a) Graph of Lattice constant vs Ni concentration (b) Graph of Crystalline size vs Ni concentration (c) Graph of Lattice strain vs Ni concentration	46
Figure 26: Carl Ziess Scanning Electron Microscope and Sputter coater setup.....	47
Figure 27: SEM images (200 nm) of a) $Ni_{0.8}Cu_{0.2}Fe_2O_4$ b) $Ni_{0.6}Cu_{0.4}Fe_2O_4$ c) $Ni_{0.4}Cu_{0.6}Fe_2O_4$ d) $Ni_{0.2}Cu_{0.8}Fe_2O_4$ e) $NiFe_2O_4$	49
Figure 28 : LabRAM HR Evolution Raman Microscope	49
Figure 29: Raman spectra of prepared samples a) $NiFe_2O_4$ b) $Ni_{0.8}Cu_{0.2}Fe_2O_4$ c) $Ni_{0.6}Cu_{0.4}Fe_2O_4$ d) $Ni_{0.4}Cu_{0.6}Fe_2O_4$ e) $Ni_{0.2}Cu_{0.8}Fe_2O_4$	52
Figure 30: Network Analyser Set-up	52
Figure 31: Set up of a pelletizer.....	53
Figure 32: Plot of Dielectric constant vs Log F(Hz) a) $NiFe_2O_4$ b) $Ni_{0.8}Cu_{0.2}Fe_2O_4$ c) $Ni_{0.6}Cu_{0.4}Fe_2O_4$ d) $Ni_{0.4}Cu_{0.6}Fe_2O_4$ e) $Ni_{0.2}Cu_{0.8}Fe_2O_4$	56

ABSTRACT

The present investigation is focused on structural, morphological and electrical properties of Nickel Copper ferrite with composition $\text{Ni}_x\text{Cu}_{1-x}\text{Fe}_2\text{O}_4$ with $x = 0.2, 0.4, 0.6, 0.8,$ and 1 were synthesised using Auto-combustion method. The samples were characterized using X-ray diffraction (XRD) for structural confirmation. The morphological study was examined using scanning electron microscope. The alteration in tetrahedral and octahedral site¹ of these nanoparticles was investigated using Raman spectroscopy. The Network analyzer was used to probe the variation dielectric constant. Nickel Copper ferrite nanoparticles can have applications in electronic devices like gas sensors. For enhancing the applicative properties of nickel copper ferrite nanoparticles further studies are required.

CHAPTER 1- INTRODUCTION

For last many decades, thin film sensor methods have been used in sensor technology, getting the attention of scientists. Thin film technology has many applications in various technological fields, offering many benefits for both the environment and humanity. Gas sensors, in particular, are highly advantageous technology that not only helps humans but also plays a important role in monitoring environmental and health conditions on a large scale.

Important part of any sensor system lies in its sensing element, and current researches aims to develop good sensors compared to those already available in the market, focusing on factors such as selectivity and sensitivity. Now making most sensitive sensing layer demands lot of research and development and this is where the significant advantages of using thin film for constructing the sensing layer become apparent. The process involved in growing thin film provide many parameters to manipulate. To make sensor systems more affordable, portable, and applicable for monitoring specific gas molecules, several criteria must be met like low power consumption for operation, compatibility with sampling systems, independence from external carrier or reactant gases, miniaturization, and lastly compatibility with microelectronic technology.[1,8]

1 NANOMATERIALS

1.1 What are nanomaterials?

Nanoscale materials or in other words nanomaterials are defined as a set of substances which have at least one dimension is less than 100 nanometers. Nanomaterials at this scale have unique optical, magnetic, electrical, and other properties.

These various emerging properties have the potential for great impacts in electronics, medicine, and other fields.

1.2 Classification of Nanomaterials:

Nanomaterials can be nanoscale in one dimension (eg. surface films), two dimensions (eg. strands or fibres), or three dimensions (eg. particles). They can exist in single, fused, aggregated or agglomerated forms with spherical, tubular, and irregular shapes. Common types of nanomaterials include nanotubes, dendrimers, quantum dots and fullerenes. Nanomaterials have applications in the field of nano technology, and displays different physical chemical characteristics from normal chemicals (i.e., silver nano, carbon nanotube, fullerene, photocatalyst, carbon nano, silica). According to Siegel, Nanostructured materials are classified as Zero dimensional, one dimensional, two dimensional, three dimensional nanostructures.

Nanomaterials can be in nanoscale in one dimension like surface films, two dimensions like strands or fibres, or three dimensions like particles. They can appear singly, fused, aggregated, or agglomerated, taking shapes like spherical, tubular, or a irregular form. Common examples of nanomaterials include nanotubes, quantum dots, and fullerenes. These nano materials find diverse applications in nanotechnology, showing distinct physical and chemical properties compared to conventional chemicals (e.g., silver nano, carbon nanotube, fullerene, photocatalyst, carbon nano, silica).

Siegel classifies nanostructured materials into zero-dimensional, one-dimensional, two-dimensional, and three-dimensional nanostructures.

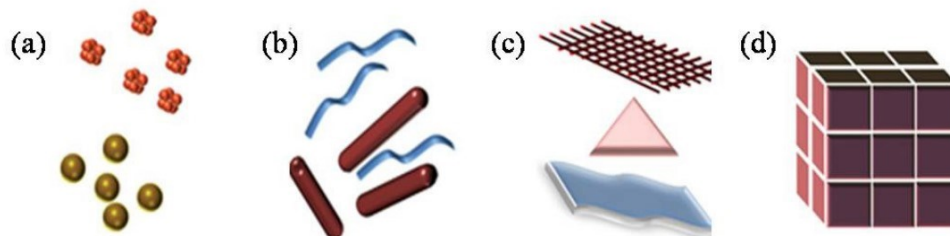


Figure 1 : Classification of Nanomaterials a) 0D spheres and clusters b) 1D nanowires, nanofibers and nanorods c) 2D nanofilms, nanoplates and networks d) 3D nanomaterials.[8]

1.3 Why so much interest in nanomaterials?

Nanomaterials have created a high interest in recent years because of their unusual and different mechanical, electrical, optical and magnetic properties. Like, Nanophase ceramics have special significance due to their increased ductility at high temperatures compared to coarse-grained ceramics, nanostructured semiconductors shows diverse nonlinear optical properties. Semiconductor quantum particles, or Q-particles, exhibit quantum confinement effects, resulting in unique properties such as luminescence observed in silicon powders and silicon germanium quantum dots, making them suitable for infrared optoelectronic devices. Nanostructured metal-oxide thin films have gained interest for developing gas sensors with improved sensitivity and selectivity. They also find application in rechargeable batteries for automobiles or consumer products. Nanocrystalline silicon films are utilized for highly transparent contacts in thin-film solar cells, while nanostructured titanium oxide porous films are employed for their high transmission and significant surface area enhancement, resulting in strong absorption in dye-sensitized solar cells.

1.4 Properties of Nanomaterials

Materials with nanometer dimensions have several key factors such as a large fraction of surface atoms, high surface energy, spatial confinement, and reduced imperfections compared to bulk materials. Due to their small size, nanomaterials possess exceptionally high surface area-to-volume ratio. These surface atoms give material properties that are heavily dependent on surface characteristics. Particularly when nanomaterial sizes approach certain thresholds, surface properties influence the entire material, potentially enhancing or altering bulk material properties. Metallic nanoparticles serve as highly active catalysts, while chemical sensors employing nanoparticles and nanowires demonstrate increased sensitivity and selectivity. Likewise, the nanometer-scale features of nanomaterials introduce spatial confinement effects, resulting in quantum effects that further influence material behavior.

1.4.1 Optical properties

The optical properties of nanomaterials are influenced by various factors such as size, shape, surface characteristics, doping, and interactions with the surrounding environment or other nanostructures. In particular, shape plays an important role in determining the optical properties of metal nanostructures. There is a notable difference in the optical properties of metal and semiconductor nanoparticles. In the case of CdSe semiconductor nanoparticles, even a small change in size can lead to significant changes in their optical properties. On the other hand, enlarging metal nanoparticles results in only minor shifts in their optical properties, as seen in various samples of gold nanospheres. However,

when introducing anisotropy to nanoparticles, such as through the growth of nanorods, the optical properties undergo significant changes.

1.4.2 Electrical Properties

The electrical properties of nanoparticles vary across different nanomaterials, such as nanotubes and nanorods, carbon nanotubes, and nanocomposites. Nanotubes and nanorods show unique electrical conductivity characteristics due to their one-dimensional nature, which leads to quantum confinement effects. Carbon nanotubes demonstrate exceptional electrical conductivity attributed to their unique structure and electronic properties. Photoconductivity, a phenomenon observed in nanorods which refers to the increase in electrical conductivity upon exposure to light, offering applications in photodetection and optoelectronics. When mechanically thinning a nanowire and measuring the electrical current at a constant applied voltage, as the diameter of the wire decreases, number of electron wave modes contributing to electrical conductivity decreases in well-defined quantized steps. This phenomenon shows the quantum mechanical nature of electron transport in nanoscale systems.

1.5 Application of nanomaterials

Nanomaterials having wide range of applications in the field of electronics, fuel cells, batteries, agriculture, food industry, and medicines, etc

Elimination of Pollutants- Nanomaterials have very large grain boundaries compared to their grain size, resulting in superior chemical, physical, and

mechanical activity. This enhanced chemical activity enables nanomaterials to serve as catalysts, reacting with harmful gases like carbon monoxide and nitrogen oxide found in automobile catalytic converters and power generation equipment. nanomaterials play a crucial role in mitigating environmental pollution caused by the combustion of gasoline and coal..

Sun-screen lotions - an extended exposure to ultraviolet (UV) radiation can lead to skin burns and an increase the risk of cancer. Sunscreen lotions having nano-TiO₂ offer improved sun protection factor (SPF) without leaving a sticky residue. Nano skin blocks, containing compounds like ZnO and TiO₂, provide an added advantage by forming a very good protective layer on the skin's surface rather than being absorbed. This barrier effectively blocks UV radiation for an extended period of time .

Sensors- depend on highly reactive surfaces to trigger a response to even very small changes in the concentration of the target species. Engineered monolayers, which are only of few Angstroms thick, are placed on the sensor surface and exposed to the surrounding environment and its distinctive functionality is used [2].

2. FERRITES

Ferrite are made up of iron oxide and metals which are ceramic materials. Ferrites are known to be hard, brittle and their colour is generally grey or black or brown. Ferrites are polycrystalline (large number of small crystals). They are written by the formula MFe_2O_4 , where M is any metal that form divalent bonds.[8]

2.1 Classification based on magnetic properties

Soft ferrites- Soft ferrites show a magnetization curve characterized by a steep rise, a narrow hysteresis loop, and minimal energy losses during magnetization. These materials are produced through a process involving heating followed by slow cooling, resulting in their ability to be easily magnetized and demagnetized. Soft ferrites are ceramic insulators with a cubic crystal structure. Due to their properties, soft ferrites possess high susceptibility and permeability, low eddy current losses, as well as low retentivity and coercivity. As a result, they find application in various fields including electromagnets, computer data storage, transformer cores, telephone signal transmitters and receivers, and more.

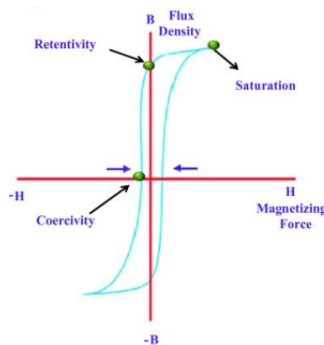


Figure 2 : B-H curve of soft ferrites [3]

Hard ferrites- referred to as permanent magnetic materials, possess the ability to retain their magnetism even after being magnetized. These ferrimagnetic materials are characterized by a magnetization curve with gradually rising slope, large hysteresis loop, and energy losses during magnetization. They are typically produced through a process involving heating followed by rapid cooling and are resistant to easy magnetization and demagnetization.

In terms of their properties, hard ferrites exhibit high saturation flux density, low susceptibility and permeability, high eddy current losses, as well as high retentivity and coercivity. These properties make them suitable for applications requiring stable and long-lasting magnetic properties, such as in permanent magnets used in various industries.

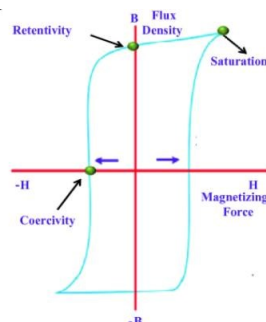


Figure 3 : B-H curve of Hard ferrites. [3]

2.2 Classification based on crystal structure

Ferrites have general formula MFe_2O_4 where M can be replaced by divalent ions like Fe^{2+} , Mg^{2+} , Co^{2+} , Ni^{2+} , Zn^{2+} , Mn^{2+} . They have two interstitial sites 1) Tetrahedral A and 2) Octahedral B. Spinel ferrites are classified basically into Normal Spinel and inverse spinel.

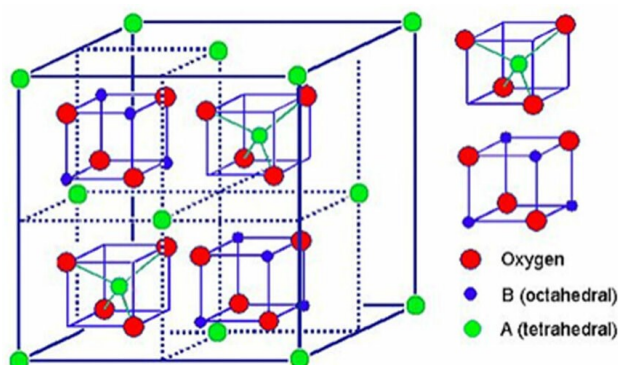


Figure 4: The spinel structure of ferrites indicating the tetrahedral and octahedral sites. The divalent AII cations occupy 1/8th of the tetrahedral voids, whereas the trivalent BIII cations occupy one half (1/2) of octahedral voids[5].

2.2.1 Normal Spinel Ferrite

General formula AB_2O_4 , where A site - divalent metal ions surrounded by 4 O^{2-} ions in tetrahedral coordination and B site – trivalent metal ions surrounded by 6 O^{2-} ions octahedrally. Eg: $(Zn^{2+})O(Fe^{3+})O_3$.

2.2.2 Inverse Spinel Ferrite

General formula AB_2O_4 , where A site – Fe^{3+} ions distributed equally in tetrahedral coordination and B site – divalent metal and Fe^{3+} ions distributed octahedrally. Arrangement: $(Fe^{3+})[Fe^{3+} Me^{2+}]O_4$. Examples are Manganese, copper and nickel ferrites.

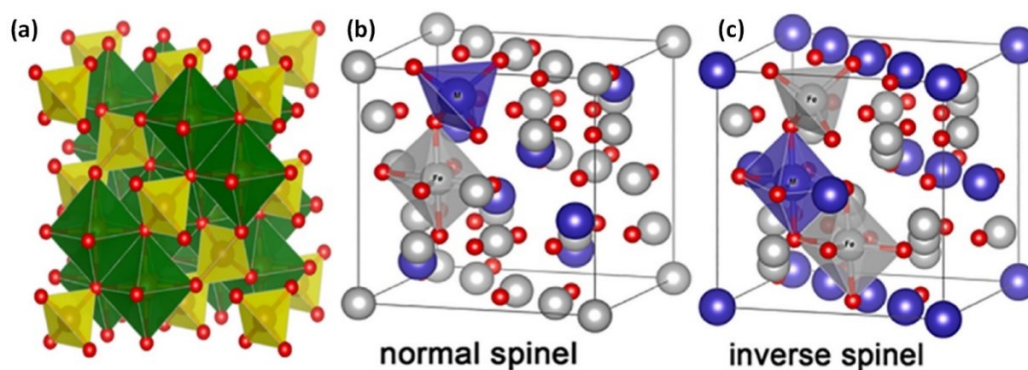


Figure 5: Structure of magnetic spinel ferrite showing tetrahedral sites (yellow), octahedral sites (green), and oxygen atoms (red) units (a) Unit cell structure of (b) normal spinel ferrite, and (c) inverse spinel ferrite.[4]

In mixed spinel structure, A^{2+} and Fe^{3+} cations randomly occupy both sites tetrahedral as well as octahedral, as seen in structures like $MgFe_2O_4$ and $MnFe_2O_4$.

2.3 Properties

The properties of ferrites make them very much suitable for a wide range of applications. The magnetic properties are from the spin moment of unpaired 3d electrons of transition elements. They exhibit electrical conductivity, Curie temperature, and magnetic crystalline anisotropy. Electrical conductivity in ferrites arises due to the hopping of electrons between ions of the same element, distributed randomly in sub-lattices with more than one valence state for example iron is present as Fe^{2+} and Fe^{3+} . The Curie temperature of ferrites tells the strength of interaction between cations at different sites which are A-site and B-site.

Magnetic properties are generally dependent on interaction between Fe^{3+} ions and can be altered by introducing dopants like rare earth metal ions into the spinel lattice, thereby affecting magnetization and Curie temperature. Spinel ferrites (SFs) have got unique properties and find applications in various fields such as high-density data storage, catalysts, gas sensors, rechargeable lithium batteries, information storage systems, magnetic cores, magnetic fluids, microwave absorbers, medical diagnostics, and therapy. In the nanoscale regime, most SFs show superparamagnetic (SPM) properties, particularly when their diameter is below or around 20 nm.[6] The properties of SFs, including structural, magnetic, electronic, and optical characteristics, are significantly enhanced in the nanoscale regime due to reductions in crystallite size and increases in specific surface area. Moreover, the size and shape of SFs can influence their physical and chemical properties, making them versatile materials for various applications.[7]

REFERENCES

1. Njoroge MA, Kirimi NM, Kuria KP. Spinel ferrites gas sensors: a review of sensing parameters, mechanism and the effects of ion substitution. *Critical Reviews in Solid State and Materials Sciences*. 2022 Nov 2;47(6):807-36.
2. A, Alagarasi,. (2011). Chapter - INTRODUCTION TO NANOMATERIALS.
3. Ajitanshu Vedrtam, Kishor Kalauni, Sunil Dubey, Aman Kumar. A comprehensive study on structure, properties, synthesis and characterization of ferrites[J]. *AIMS Materials Science*, 2020, 7(6): 800-835.
4. Mapossa AB, Mhike W, Adalima JL, Tichapondwa S. Removal of organic dyes from water and wastewater using magnetic ferrite-based titanium oxide and zinc oxide nanocomposites: a review. *Catalysts*. 2021 Dec 18;11(12):1543.
5. Njoroge, Muasya & Kirimi, Nixon & Kamweru, Paul. (2021). Spinel ferrites gas sensors: a review of sensing parameters, mechanism and the effects of ion substitution. *Critical Reviews in Solid State and Materials Sciences*. 47. 1-30. 10.1080/10408436.2021.1935213.
6. Singh A, Singh A, Singh S, Tandon P, Yadav BC. Preparation and characterization of nanocrystalline nickel ferrite thin films for development of a gas sensor at room temperature. *Journal of Materials Science: Materials in Electronics*. 2016 Aug;27:8047-54
7. Vedrtam A, Kalauni K, Dubey S, Kumar A. A comprehensive study on structure, properties, synthesis and characterization of ferrites. *AIMS Materials Science*. 2020;7(6):800-35.
8. <https://ebooks.inflibnet.ac.in/msp12/chapter/thin-film-gas-sensing-application/>.

CHAPTER 2 – LITERATURE REVIEW

Cao GX et al. synthesized nano sized copper ferrite using $\text{Cu}(\text{NO}_3)_2 \cdot 3\text{H}_2\text{O}$, $\text{Fe}(\text{NO}_3)_3 \cdot 9\text{H}_2\text{O}$, and malic acid as raw materials through the auto-combustion process under lower temperature with short time. Copper ferrite was directly formed after auto-combustion of the dry-gel precursor, and did not require more calcination at high temperature. The precursor decomposed completely at about 199°C and yield single phase product. TEM results showed that nano-particles show narrow size distribution and mainly show sphericity. This method can be used in the industry due to its simpleness, economy and high quality.[1]

Sagadevan S et al. synthesized NiFe_2O_4 nanoparticles by using co-precipitation method. XRD data showed NiFe_2O_4 nanoparticles belonged to the cubic spinal structure. FTIR spectrum also showed the formation of NiFe_2O_4 nanoparticles. SEM analysis showed that the nanoparticles agglomerated to form spherical-shaped particles. The average particle size of nanoparticles was found to be 28 nm. The impact of the frequency and the temperature on the dielectric loss and the dielectric constant for NiFe_2O_4 nanoparticles were studied. From the dielectric studies it became clear that the frequency negatively impacted both the dielectric constant and the dielectric loss as decreased with increase in the frequency. A study of the magnetic properties was also done using VSM measurements. [2]

Lassoued A et al. synthesized single phase Ni & Cu ferrites and its solid solutions. Cu doped NiFe_2O_4 of the type $\text{Cu}_x\text{Ni}_{1-x}\text{Fe}_2\text{O}_4$ prepared by the co-precipitation method. The synthesized Ni–Cu ferrite at different copper concentration is characterised by XRD, TEM, SEM, FTIR, Raman, TGA, DTA, UV–Visible and VSM. The X-ray diffraction studies clearly showed the formation of single phase spinel structure and the particle

size beyond the nanoscale. The lattice parameter is found to be increasing copper content. TEM and SEM observations shows cubic-shaped nanoparticles of $\text{Cu}_x\text{Ni}_{1-x}\text{Fe}_2\text{O}_4$. The crystalline particle size was found to be in the range of ~ 14 to ~ 43 nm. The FT-IR spectroscopy study shows two main metal oxygen bonds in the range of $400\text{--}600\text{ cm}^{-1}$ confirming the formation of single phase cubic inverse structure of Cu substitute Ni ferrite. The Raman spectra shows five Raman active modes ($A_{1g}+E_g+3F_{2g}$) which are expected in the spinel structure and Raman spectra has a very good agreement with reported data. The optical study showed that the samples has optical band gap between 1.77 and 1.59 eV. From the hysteresis loop, it was clear that synthesized sample can be control, for the Cu^{2+} substituted in Ni ferrite. [3]

Anjum S et al. synthesized NiCu ferrites with the general formula $\text{Ni}_{1-x}\text{Cu}_x\text{Fe}_2\text{O}_4$, where $x = 0, 0.2, 0.4, 0.6, 0.8$, by double-sintering method. The single-phase spinel structure is confirmed by XRD. This analysis showed the increasing lattice parameter due to the larger ionic radii of the Cu ion. Fourier transform infrared spectra confirmed the two prominent bands of spinel ferrites in the range $1000\text{--}400\text{ cm}^{-1}$. Magnetic properties were studied using vibrating sample magnetometer. It was investigated that the saturation magnetization decreases linearly as the copper concentration increases. The surface morphology is shown using SEM. The dielectric properties have been investigated as a function of frequency. As the dielectric constant is decreased and ac conductivity is increased at higher frequency.[4]

Mahalakshmi S et al. synthesized Copper-Doped Nickel Ferrite. XRD patterns confirmed the formation of single-phased cubic spinel structure without any of the impurity. The SEM images shows that the particle size of the particles lies in the nanometer range. The particle sharpness is more or less spherical with some cluster/agglomeration between the particles. The lattice parameter is varied with the

increase of Cu content in the mixed NiCu ferrite system due to the larger ionic radius of octahedral sites.[5]

Sultan M et al. synthesized $\text{Cu}_{0.6}\text{Zn}_{0.4}\text{Fe}_2\text{O}_4$ thin films using rf-magnetron sputtering on glass substrates at room temperature in pure Argon gas environment. The influence of variation in Argon gas pressure between 5 and 15 mT on the crystal structure and magnetization has been studied. The XRD patterns showed single phase nanocrystalline spinel structure with cubic symmetry. The AFM images confirms the nanocrystalline nature of the films. The magnetization increases with increase in Ar gas pressure. The change in crystal structure and magnetization has been explained in view of freezing of some Cu-ions on tetrahedral A-sites and equivalent number of Fe ions on octahedral B-sites during the deposition process due to high deposition rate in pure Ar environment.[6]

Samarasekara P et al. studied the properties of sputtered polycrystalline Ni ferrite ($\text{NiO}:\text{Fe}_2\text{O}_3$) films in detail. All these films were sputtered on Al_2O_3 polycrystalline substrates. The coercivity of the films drastically increased from 5 to 800 Oe as the deposition temperature was raised from 60 to 600°C. Polycrystalline ferrite films with higher coercivity are useful for high-density recording media. It is difficult to directly or subsequently (with annealing) deposit aligned (or oriented) films of Ni ferrite on polycrystalline substrates according to our studies. The X-ray diffraction patterns, scanning electron microscope (SEM) measurements and magnetic measurements were performed for these Ni ferrite films.[7]

Manikandan V et al. synthesized Nano crystalline structured tin substituted nickel ferrite thin film prepared by chemical coprecipitation method and thin films using spin coating. XRD analysis reveals the average crystallite size as 51 nm and most

preferential peak (311) confirms the formation of tin substituted nickel ferrite. The SEM morphology shows the large number of active sites. UV analysis, it was observed that material has absorption in visible region at ~ 201 nm. Humidity sensing analysis show highly sensitive towards humidity, excellent stability over a long time and good response and recovery times.[8]

Singh A et al. fabricated LPG sensor based on nanocrystalline NiFe_2O_4 thin film using the spin coating process. The structural and surface morphological properties of the fabricated films were studied by X-ray diffraction (XRD) and scanning electron microscopy. The prepared films were exposed to the target gases and their temporal variations in electrical resistance for different concentrations of LPG were recorded using a Keithley electrometer (Model—6514). The sensing results show that the fabricated sensor is challenging for the leakage detection of LPG as it possesses high sensitivity, stable behavior and small response and recovery times towards LPG.[9]

Rao P et al. fabricated NiFe_2O_4 and (1 wt% and 3 wt%) $\text{Cu}:\text{NiFe}_2\text{O}_4$ thin films using spray pyrolysis deposition technique. XRD revealed that all samples had shown the principal phase of nickel ferrite and the lattice parameter was found to vary from 8.294 Å to 8.314 Å on an incorporation of Cu. SQUID VSM were carried out to investigate influence of Cu doping on magnetic properties. Gas response towards various gases Ethanol, Liquid Petroleum Gas (LPG), methanol and hydrogen sulfide. The sensor based on NiFe_2O_4 thin films showed selective response towards 5 ppm of ethanol at operating temperature 375 °C which shifts towards much lower temperature 325 °C for $\text{Cu}:\text{NiFe}_2\text{O}_4$ thin films as compared to other gases.[10]

REFERENCES

1. Cao GX, Liu T, Zhang QH, Wang HZ. Synthesis and characterization of nanometer copper ferrite by auto-combustion. *Advanced Materials Research*. 2012 Jan 9;347:3472-6.
2. Sagadevan S, Chowdhury ZZ, Rafique RF. Preparation and characterization of nickel ferrite nanoparticles via co-precipitation method. *Materials Research*. 2018 Jan 22;21:e20160533.
3. Lassoued A, Lassoued MS, Karolak F, García-Granda S, Dkhil B, Ammar S, Gadri A. Synthesis, structural, optical, morphological and magnetic characterization of copper substituted nickel ferrite ($\text{Cu}_x\text{Ni}_{1-x}\text{Fe}_2\text{O}_4$) through co-precipitation method. *Journal of Materials Science: Materials in Electronics*. 2017 Dec;28:18480-8.
4. Anjum S, Rashid A, Bashir F, Riaz S, Pervaiz M, Zia R. Effect of Cu-doped nickel ferrites on structural, magnetic, and dielectric properties. *IEEE Transactions on Magnetics*. 2014 Aug 20;50(8):1-4.
5. Mahalakshmi S, Srinivasa Manja K, Nithiyantham S. Structural and morphological studies of copper-doped nickel ferrite. *Journal of Superconductivity and Novel Magnetism*. 2015 Oct;28:3093-8.
6. Sultan M, Singh R. Crystal structure and magnetic properties of rf-sputtered Cu–Zn ferrite thin films. *Journal of Applied Physics*. 2010 May 1;107(9).
7. Samarasekara P, Cadieu FJ. Polycrystalline Ni ferrite films deposited by RF sputtering techniques. *Japanese Journal of Applied Physics*. 2001 May 1;40(5R):3176.
8. Manikandan V, Sikarwar S, Yadav BC. Fabrication of Tin substituted Nickel Ferrite.

9. Singh A, Singh A, Singh S, Tandon P, Yadav BC. Preparation and characterization of nanocrystalline nickel ferrite thin films for development of a gas sensor at room temperature. *Journal of Materials Science: Materials in Electronics*. 2016 Aug;27:8047-54.
10. Rao P, Godbole RV, Bhagwat S. Copper doped nickel ferrite nano-crystalline thin films: a potential gas sensor towards reducing gases. *Materials Chemistry and Physics*. 2016 Mar 1;171:260-6.

Chapter 3 - METHODS OF SAMPLE PREPARATION

3.1 Methods available for Ferrite nanopowder preparation

3.1.1 Co-precipitation Method

The synthesis of spinel ferrites by coprecipitation method is most convenient, economic, and less time-consuming, has high mass production, and is frequently employed among all other methods in order to get uniform-sized nano particles. In co-precipitation method, reactants are taken in the form of chlorides or nitrates and mixed in distilled water and then suitable precipitating agent such as hydroxides is added as to get precipitates. The precipitates are uniform mixture of reactants in the form of ferrite metals on the atomic scale. The precipitates are washed to remove the impurities and separated from the mother liquid with the help of centrifuge.[1]

The obtained precipitates are dried in hot oven to burn the carbonaceous matter leaving a residue of ferrite metals. The residue is then grinded to obtain powder. For the growth of suitable nanoparticles pre-sintering and sintering is done at suitable temperature. This method is also commonly used to synthesize biocompatible SFs.

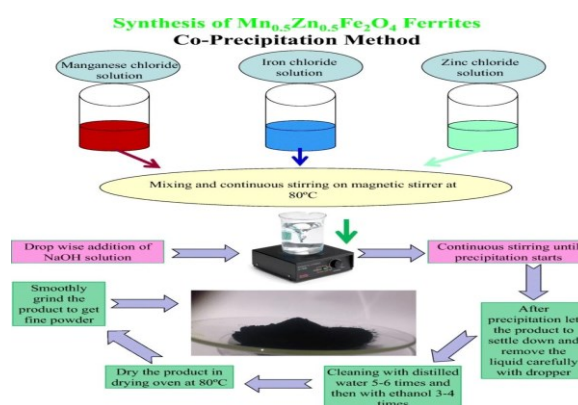


Figure 6: schematic diagram of processes involved in co-precipitation method[1]

3.1.2 Auto-Combustion Method

Auto combustion is also known as self-propagating high temperature synthesis since the desired inorganic material is formed by exothermic combustion reactions. It follows a process of bringing a saturated aqueous solution of the desired metal salts and a suitable organic fuel to boil, until the mixture ignites and rather faster combustion reaction takes off, resulting in a dry, usually crystalline and fine particle oxide powder. To produce a mixed oxide, the mixture containing the desired metal ions, in the form of water-soluble nitrate salts and a fuel such as urea can be used. A constant external heat supply is necessary in this case, to maintain the system at the high temperature required to accomplish the phase transformation temperature.

In auto-combustion method firstly metal nitrite/acetate are weighed and added in distilled water. Urea is added for Combustion and then NTA is added to this mixture which help in the combustion process. Solution obtained is then mixed well with the help of magnetic stirrer during which it is kept on hot plate. The solution obtained is then poured on the plate and mixed throughly on the hot plate till all the solvent is evaporated. After the drying stage, the produced material is then grinded for 15 minutes to get the desired nanopowder.

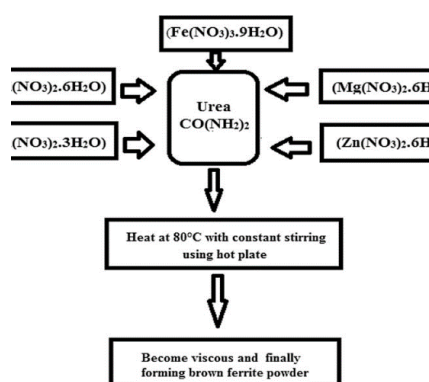


Figure 7: Flow chart of processes involved in auto combustion[2].

3.1.3 Hydrothermal Method

Hydrothermal synthesis is a method of producing materials by using high-pressure and high-temperature aqueous solutions. Water acts as both the solvent and the reaction medium, facilitating the formation of various compounds. The hydrothermal environment allows for the synthesis of materials with unique properties and structures that are not easily achievable under standard conditions. The solubility of reactants and products in water varies with temperature and pressure, influencing the formation of different materials.[3,4]

This involves heating of the reactants in a close vessel called Autoclave, autoclave is usually constructed from thick stainless steel to withstand the high pressure and is fitted with a safety wall. It may be lined with Teflon (Non reactive material). When autoclave is heated the pressure increases and the water remains liquid above its normal boiling temperature of 373 K which is called superheated water. These conditions when pressure is raised above atmospheric pressure and temperature above the boiling temperature are known as "Hydrothermal method".[5]

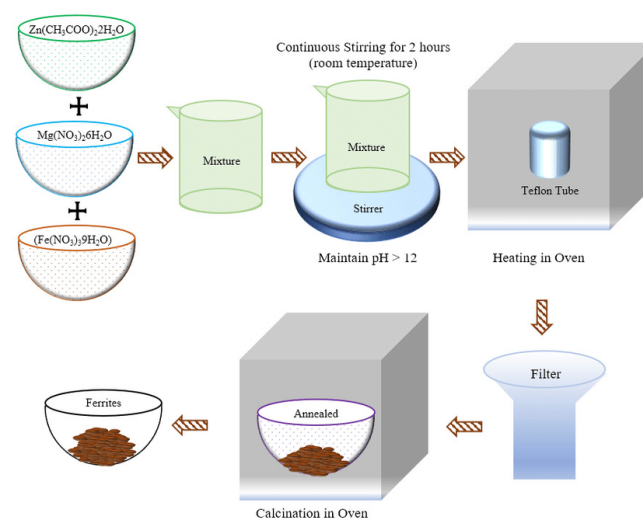


Figure 8: The flowchart for synthesis of ferrite via hydrothermal method.[6]

3.2 Methods available for Thin Films preparation

Two common deposition techniques:

- **Chemical deposition:** A fluid precursor undergoes a chemical change at a solid surface, leaving a solid layer.
- **Physical deposition:** Uses mechanical, electromechanical or thermodynamic means to produce a thin film of solid.

3.2.1 Chemical deposition

a) Spin Coating

Spin coating is a method to prepare uniform and homogeneous thin films onto the flat substrates. Spin coater works on the principal of centrifugal force. The machine used here is commonly called spin coater or spinner. The working of this technique is divided in 4 steps deposition:- spin up, spin down and evaporation.[7]

- i. Deposition – The solution is put on the centre of substrate with the help of pipette. It has to be put in such way that no bubbles are formed.
- ii. Spin-up – during this process the substrate is spun at high rpm and because of centrifugal force the solution will uniformly spread out on the substrate. Usually 1000-6000 rpm. Here most of the solution is expelled out and it becomes thin layer because of viscous force.
- iii. Spin-down – The transition to this process is not abrupt, the speed is reduced slowly and colour of the fluid starts changing indicating that evaporation of solvent has started.

- iv. Evaporation – Here evaporation increases because of increase in viscous forces. The fluid outflow is stopped. The rate of evaporation is determined by solvent volatility.

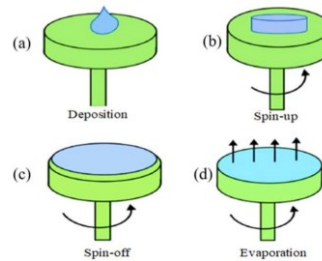


Figure 9: Spin coating various stages.[7]

b) Spray pyrolysis

A simple and inexpensive method of synthesizing thin and thick film, metal and metal oxide coating in large scale. An aerosol process that atomizes a solution and heats the droplets to produce solid particles. Pyro=heat and lysis=breaking, pyrolysis-change under the action of heat. Spray pyrolysis method is based on forming an aerosol from various precursor solutions, which could be a solution of metallic salts or a colloidal solution. The generated solution droplets (aerosol) are then rapidly heated in a furnace at given temperature, thus passing through several stages: (1) evaporation of the solvent from the surface of the droplets, (2) drying the droplets containing the precipitated solute, (3) the annealing of the precipitate at high temperatures (thermolysis), (4) formation of microporous particles of defined phase composition, (5) formation of solid particles, and (6) sintering of solid particles. The particles obtained after thermolysis are very reactive and hence inner (“in situ”) sintering is needed. In this procedure, preparation of uniform and fine droplets of reactants and their controlled thermal decomposition are demanding operations

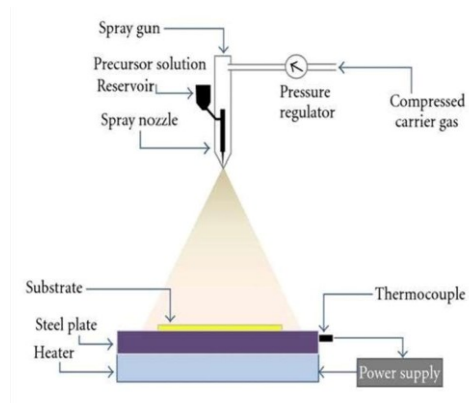


Figure 10: Schematic diagram of Spray Pyrolysis Method.[9]

3.2.2 Physical deposition

a) Sputtering Method

In this method of depositing thin films a gaseous plasma is generated by applying an electric field inside a vacuum chamber filled with a heavy inert gas such as Argon, at a specific pressure. The inert gas ions accelerate under the field towards the cathode which is made of the source material (called the target). Momentum transfer from the bombarding ions to the surface atoms of the target results in their ejection. The ejected atoms diffuse towards the substrate (attached to the anode) and are deposited.

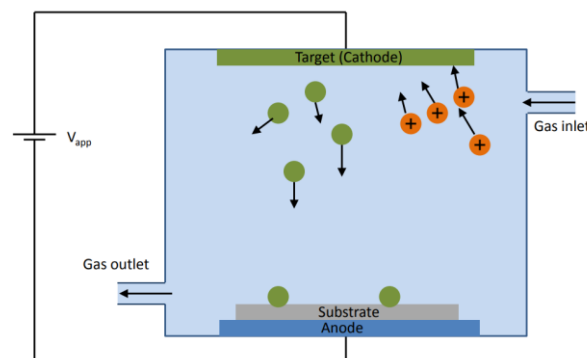


Figure 11: Schematic diagram of Sputtering.[8]

RF Sputtering

Instead of applying a DC voltage to the cathode, apply voltage oscillating at radio frequency (RF), typically around 13.5 MHz. The RF peak to peak voltage is around 1000V, electron densities are around 10^9 - 10^{11} cm^{-3} and the chamber pressure is 0.5 -10 mTorr. On the positive cycle, electrons are attracted to the cathode, creating a negative bias (think of it as replenishing the negative charge on the target surface). On the negative cycle ion bombardment continues.

Advantages

- It helps in deposition of wide variety of insulators, metals, alloys, composites etc. It Works well for insulating targets.
- Charge-up effects are avoided and arcing is reduced due to use of AC RF source of frequency 13.56 MHz. This is due to the fact that electric field sign at every surface inside plasma chamber changes with RF.
- It can operate at low pressures (1 to 15 mTorr) while sustaining plasma. Hence RF sputtering offers higher efficiency.
- This sputtering technique is used to sputter any type of film.

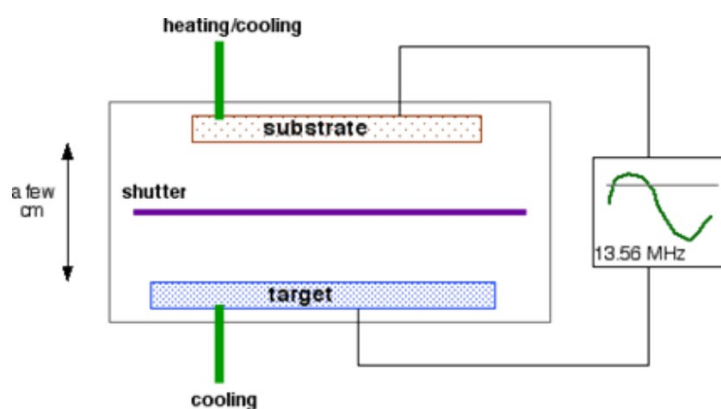


Figure 12:Schematic diagram of RF Sputtering.[10]

b) Pulsed laser Deposition (PLD)

PLD is a deposition technique where a high-power pulsed laser beam is focused inside a vacuum chamber to strike a target of the material that is to be deposited. This material is vaporized from the target (in a plasma plume) which deposits it as a thin film on a substrate. This process can occur in ultra high vacuum or in the presence of a background gas, such as oxygen which is commonly used when depositing oxides to fully oxygenate the deposited films.

Advantages:

- Simple (fast, and easiest to study new chemical systems).
- Compatible with oxygen and other reactive gases
- The film thickness can be controlled by tuning deposition parameters.
- The high crystallinity of the prepared film.
- It provides precise transfer of stoichiometry from target to substrate.

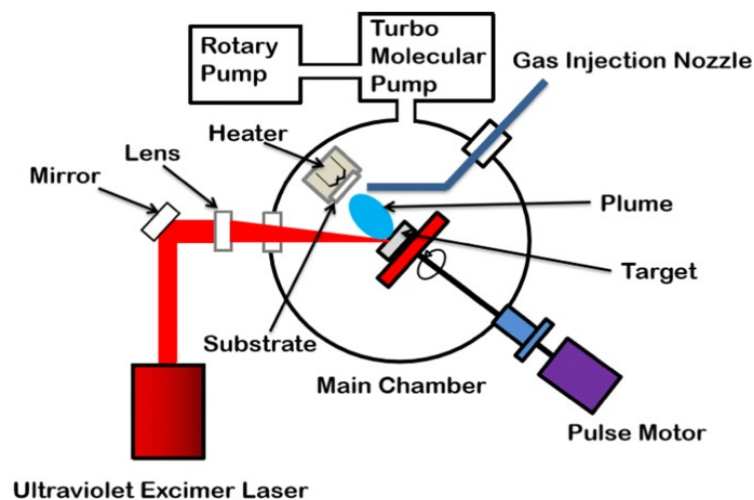


Figure 13: Schematic diagram of Pulsed Laser deposition technique. [11]

3.3 Preparation of Nickel copper ferrites by Auto-combustion method

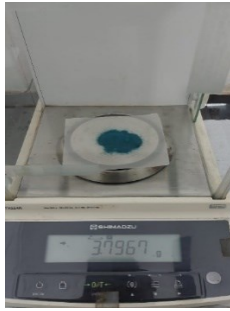
Prepared 5 samples are as follows;

1. $\text{Ni}_{0.2}\text{Cu}_{0.8}\text{Fe}_2\text{O}_4$
2. $\text{Ni}_{0.4}\text{Cu}_{0.6}\text{Fe}_2\text{O}_4$
3. $\text{Ni}_{0.6}\text{Cu}_{0.4}\text{Fe}_2\text{O}_4$
4. $\text{Ni}_{0.8}\text{Cu}_{0.2}\text{Fe}_2\text{O}_4$
5. NiFe_2O_4

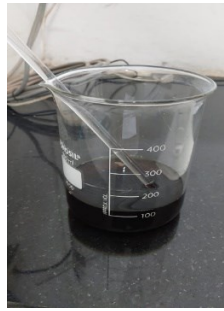
Steps involved in this method are,

- Firstly Nickel nitrate, Copper acetate and Ferric Nitrate are weighed according to their stoichiometric ratios and added in distilled water (Only for pure nickel ferrite sample only nickel acetate and ferric nitrate is added).
- Urea is added as fuel and then nitrilotriacetic acid (NTA) is added as complexing agent which facilitates combustion.
- Solution these reactants is then mixed with the help of automatic stirrer during which it is kept at an elevated temperature for volume reduction .
- After the mixture has reduced its volume to 100 ml it is then poured on the hot flat plate for further volume reduction .
- When the fuel ignition temperature is reached a dry mass is obtained, which is then crushed to get the nanopowder.

Step by step process of making nickel copper ferrite nanoparticles by Auto-combustion method.



1. weighing



2. Adding contents to distilled water



3. Stirring solution on hotplate



4. stirring manually on hot plate



5. Auto-combustion at Fuel ignition temp.



6. Crushing

Figure 14: Step by step process of making Ni Cu nanopowder by auto-combustion technique.

REFERENCE

1. Saqib M, Ali SS, Zulqarnain M, Qadri MU, Riaz M, Hasan MS, Khan MI, Tahir M, Arshad MI, Rani HS. Temperature-dependent variations in structural, magnetic, and optical behavior of doped ferrites nanoparticles. *Journal of Superconductivity and Novel Magnetism*. 2021 Feb;34:609-16.
2. Henaish, A. et.al (2020). Spectral, electrical, magnetic and radiation shielding studies of Mg-doped Ni–Cu–Zn nanoferrites. *Journal of Materials Science: Materials in Electronics*.
3. Yang, G., & Park, S.-J. (2019). *Conventional and Microwave Hydrothermal Synthesis and Application of Functional Materials: A Review*.
4. Dahiya, M. S., Tomer, V. K., & Duhan, S. (2018). 31 - Metal–ferrite nanocomposites for targeted drug delivery. *Applications of Nanocomposite Materials in Drug Delivery*.
5. MODAN, E. M., & PLĂIAȘU, A. G. (2020). Advantages and Disadvantages of Chemical Methods in the Elaboration of Nanomaterials.
6. Vedrtnam, Ajitanshu & Kalauni, Kishor & Dubey, Sunil & Kumar, Aman. (2020). A comprehensive study on structure, properties, synthesis and characterization of ferrites. *AIMS Materials Science*. 7. 800-835. 10.3934/matricsci.2020.6.800.
7. Jameel, Dier & Mustafa, Haveen. (2021). Modeling and the main stages of spin coating process: A review. *Journal of Applied Science and Technology Trends*. 2. 91-95. 10.38094/jastt203109.
8. Shi F. Introductory Chapter: Basic Theory of Magnetron Sputtering [Internet]. *Magnetron Sputtering [Working Title]*. IntechOpen; 2018.

9. Bari, Ramesh & Patil, Sharad & Bari, Dr. Anil. (2013). Spray-pyrolized nanostructured CuO thin films for H₂S gas sensor. International Nano Letters. 3. 10.1186/2228-5326-3-12.
10. <https://www.aemdeposition.com/blog/dc-sputtering-vs-rf-sputtering.html>.
11. Masood KB, Kumar P, Malik MA, Singh J. A comprehensive tutorial on the pulsed laser deposition technique and developments in the fabrication of low dimensional systems and nanostructures. Emergent Materials. 2021 Jun;4(3):737-54.

Chapter 4 – CHARACTERISATION TECHNIQUES

4.1 X-Ray diffraction

X-Ray diffraction analysis (XRD) is a non-destructive technique that provides us with detailed information about the crystallographic structure, chemical composition, and physical properties of a material. It is based on constructive interference of monochromatic X-rays and a crystalline sample. XRD works by irradiating the material with incident X-rays and then measuring the intensities and scattering angles of the X-rays that leave the material. [1,2]

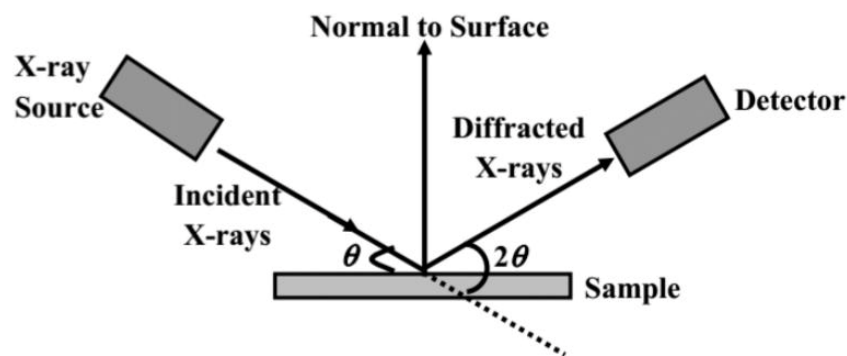


Figure 15: Schematic diagram of X-Ray Diffraction Spectroscopy. [1,2]

X-rays are generated in a cathode ray tube by heating a filament to produce electrons, accelerating the electrons toward a target by applying a voltage, and bombarding the target material with electrons. When electrons have sufficient energy to dislodge inner shell electrons of the target material, characteristic X-ray spectra are produced. These spectra consist of several components, the most common being $K\alpha$ and $K\beta$. These X-rays are collimated and directed onto the sample. As the sample and detector are rotated, the intensity of the reflected X-rays is recorded. When the geometry of the incident X-rays impinging the sample satisfies Bragg's law, constructive interference occurs and a peak in intensity appears. A detector records and processes this X-ray

signal and converts the signal to a count rate, which is then output to a device such as a printer or a computer monitor.



Figure 16: Rigaku Smart Lab X-Ray Diffractometer.

4.2 Scanning Electron Microscopy

Scanning electron microscope (SEM) is a type of electron microscope that produces images of a sample by scanning the surface with a focused beam of electrons. The electrons interact with atoms in the sample, producing various signals that contain information about the surface topography and composition of the sample.

- **Electron gun** – Produces electron cloud that will be used to look at the sample
- **Anode** – metal plate which has a positive charge. It attracts the electrons to form a beam.
- **Magnetic lens system**- made of a roll of wire that carries electricity and creates a magnetic force that directs the path of the electron beam.
- **Scanning Coils** – Scanning is done with pair of coils called Scanning coils. The Scanning coils move the sample cross the sample. These electromagnetic coils

are energized by Scan generator which is connected to the computer. This beam of electrons then strikes the sample and is reflected back.

- **Electron detector** – attracts the electrons that bounce back and turn them into electrical current.
- This electrical current is then given to computer which turns it into image on screen.

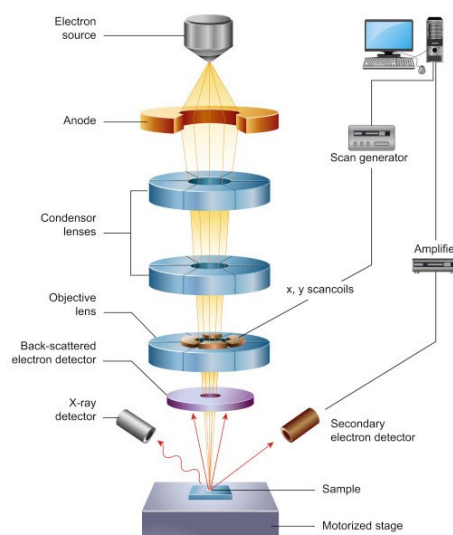


Figure 17: Schematic of a scanning electron microscope.[3]

4.3 UV-Vis spectroscopy

UV Vis spectroscopy is a scientific technique used to measure the amount of light that is absorbed or transmitted by a sample at different wavelengths of ultraviolet (UV) and visible (Vis) light [5]. Ultraviolet–visible (UV–visible) spectroscopy is primarily a quantitative analytical technique concerned with the absorption of near-UV (180–390 nm) or visible (390–780 nm) radiation by chemical species in solution. The process

involves shining a beam of UV Vis light through the sample and measuring the amount of light that passes through it. By analysing the pattern of absorption and transmission of light, we can identify and quantify the components of the sample.[4]

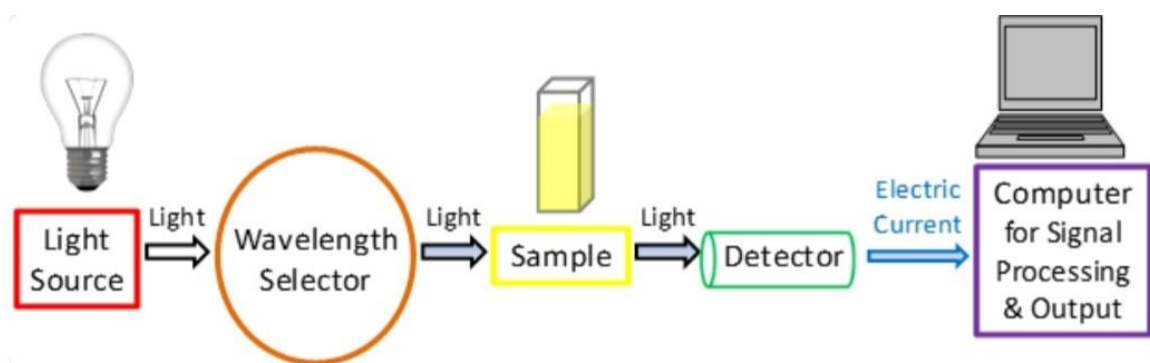


Figure 18: Schematic diagram of UV-Vis Spectrometer.[6]

4.4 Raman spectroscopy

Raman spectroscopy relies upon inelastic scattering of photons, known as Raman scattering. Raman spectroscopy belongs into the category of vibrational spectroscopy which is a powerful tool to characterize the structure of various kinds of materials. It chemically analyses the sample by using light to excite molecular vibration, and interpreting this interaction afterwards. It is based on the inelastic scattering of light that occurs when matter is irradiated by light. As the change of wavelength is very small compared to the wavelength of the irradiating light, the change of wavelength is most easily observed when using monochromatic light sources. After this monochromatic light gets interacted with the sample, a very small part of it has changed its wavelength. This is called as the Raman effect which was discovered by C.V. Raman in 1930. Raman spectroscopy did not really take off however, until the

discovery of the laser thus, the use of monochromatic light plays an important role. The sample is irradiated with a laser and some of the scattered light is analysed with a spectrograph. At the end Raman spectrum is obtained which shows the characteristic signals or “bands” for the material under investigation.

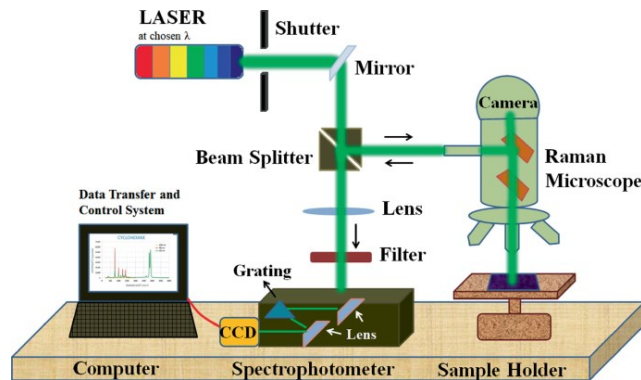


Figure 19: working of Raman spectroscopy.[10]

In Raman spectroscopy technique, the sample is irradiated with a monochromatic laser beam which interacts with the molecules of sample and originates a scattered light. This scattered light has a frequency different from that of incident light is used to construct a Raman spectrum. Raman spectra arises due to an inelastic collision between incident monochromatic radiation and molecules of sample. When a monochromatic radiation strikes at sample, it scatters in all directions after its interaction with sample molecules. Much of this scattered radiation has a frequency which is equal to frequency of incident radiation and constitutes Rayleigh scattering. Only a small fraction of scattered radiation has a frequency different from frequency of incident radiation and constitutes Raman scattering. When the frequency of incident radiation is higher than frequency of scattered radiation, Stokes lines appear in Raman spectrum. But when the frequency of incident radiation is lower than frequency of scattered radiation, anti-Stokes lines appear in Raman spectrum. Scattered radiation

is usually measured at right angle to incident radiation. [7,8] Stokes shifted Raman bands involve the transitions from lower to higher energy vibrational levels and therefore, Stokes bands are more intense than anti-Stokes bands and hence are measured in conventional Raman spectroscopy while anti-Stokes bands are measured with fluorescing samples because fluorescence causes interference with Stokes bands. The magnitude of Raman shifts does not depend on wavelength of incident radiation. Raman scattering depends on wavelength of incident radiation. A change in polarizability during molecular vibration is an essential requirement to obtain Raman spectrum of sample. Since Raman scattering due to water is low, water is an ideal solvent for dissolving samples. Glass can be used for optical components in Raman spectrophotometer. [7,8,9].

The common practice to plotting Raman spectra is intensity, or "Count Rate", on the y-axis and the frequency of the "Raman Shift" along the x-axis. Raman shift is the difference in frequency between the laser light and the scattered light. One method of interpreting Raman spectra is the recognition of molecular functional groups, which are distinct subunits of a molecule. The vibrations of functional groups appear in Raman spectra at distinctive Raman shifts. These characteristic shifts allow for an unknown compound to be linked to a known class of substances.[7,8]

4.5 Electrical Measurements

Dielectric properties - Different dielectric materials have different and unique set of electrical characteristics which depend on their dielectric properties. These properties when measured accurately can provide valuable information incorporate the material into its intended applications for more solid designs or to monitor the manufacturing

process for improved quality material. A dielectric supports charge by acquiring polarization in an electric field, whereby one surface develops a net positive charge while opposite surface develops a net negative charge. This is made possible by the presence of electric dipoles. All nonconducting materials are capable of electronic polarization hence, all insulators are dielectric to some degree. In contrast the ionic orientation modes are only available to materials possessing ions and permanent dipoles respectively. [11]

Dielectric constant - The dielectric constant of a substance or material is a measure of its ability to store electrical energy. It is an expression of the extent to which a material holds or concentrates electric flux.

Dielectric loss – an efficient dielectric supports a varying charge with minimal dissipation of energy in the form of heat. Conduction loss and dielectric loss are the two main forms of loss that may dissipate energy within a dielectric. In conduction loss a flow of charge through the material causes energy dissipation whereas dielectric loss is the dissipation of energy through the movement of charges in an alternating electromagnetic field as polarization switches direction. [11]

The as prepared nanocomposite sample was pressed into pellets of 13mm diameter and about 2mm in thickness by applying pressure of about 3 ton. Once the pellets were formed, both faces of the pellets were painted with silver for making ohmic contacts. Experimental technique and setup: The instrument used is basically an electrical network analyser that is used to measure an electrical network's network parameters. Currently, these instruments are normally used to measure S-parameters i.e., scattering parameters which describe the main relationships between input and output ports within an electrical system because transmission and reflection of

electrical networks are very simple to calculate at high frequencies, although there are other types of network parameter sets like Y, Z & H parameters. These analysers are frequently used to differentiate two-port networks like filters & amplifiers and filters. The basic working principle of a network analyser is to measure the phase & amplitude of both the waves like reflected and incident at the different ports of the Device Under Test (DUT). This analyser includes both a source & set of receivers. A source is used to produce a known stimulus signal whereas receivers are used to decide changes in stimulus signal which is caused by the DUT. Generally, a network analyser has the capacity to understand different protocols, which provides information regarding what is happening on a network by letting you observe the actual data that supplies packet by packet over it. It is used in transmission & reflection measurements. Transmission measurements comprise gain, insertion loss, transmission coefficient whereas reflection measurements comprise return loss, reflection coefficient, impedance, etc. The operating frequencies of these analysers range from 1 Hz -1.5 THz. These analysers can also be used for the analysis of stability for the measurement of ultrasonic, audio components, and open loops.

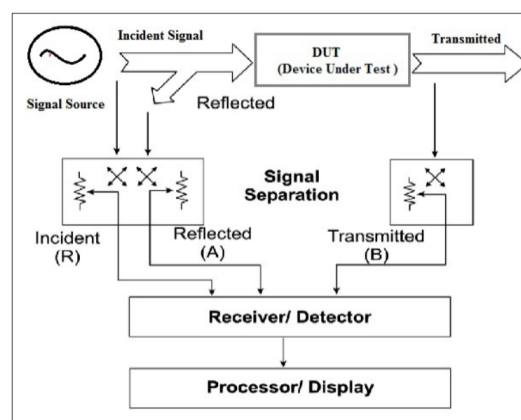


Figure 20: Block Diagram of Electrical Network Analyser



Figure 21: Electrical network analyser setup.

4.6 ATOMIC FORCE MICROSCOPY

Atomic force microscopy is an amazing technique that allows us to see and measure surface structure with very high resolution and accuracy. AFM allows us to get images showing the arrangement of individual atoms in a sample, or to see the structure of individual molecules. Working includes scanning of AFM probe with a sharp cantilever tip over the surface of the sample. The Cantilever tip is usually made up of silicon nitride which is flexible . The piezoelectric ceramic scanner helps in controlling the position of the AFM probe in both vertical and lateral directions. The cantilever tip moves over the surface measuring the different heights deflecting over the surface. The deflection is measured by the laser beam on the backside of the

cantilever tip which is directed towards the position detector. The feedback loop controls the scanner at the vertical extension to maintain the constant cantilever deflection with constant interaction force. The coordinates that are measured by the cantilever tip is used to generate the 3D topographical image of the surface.[12]

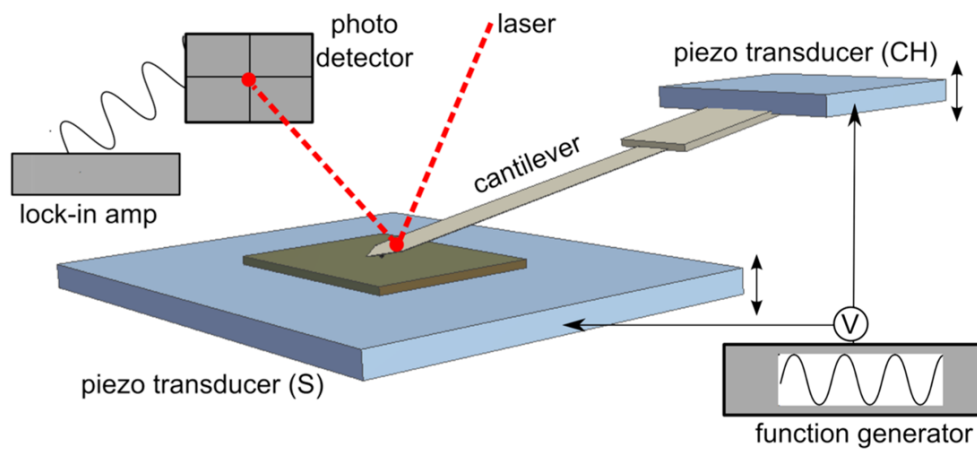


Figure 22: Schematic Diagram of Atomic Force Microscopy.[13]

REFERENCES

1. Dutrow, B. L., & Clark, C. M. (n.d.). X-ray Powder Diffraction (XRD).
2. Stanjek, H., & Häusler, W. (2004). Basics of X-ray Diffraction. Springer series in plasma science and technology.
3. <https://www.nanoscience.com/techniques/scanning-electron-microscopy/>
4. Worsfold, P. (2005). SPECTROPHOTOMETRY | Overview. Encyclopedia of Analytical Science (Second Edition).
5. Tom, J. (2023). UV-Vis Spectroscopy: Principle, Strengths and Limitations and Applications.
6. Tom, J. (2023). UV-Vis Spectroscopy: Principle, Strengths and Limitations and Applications.
7. Javier, J. (2014). An Introduction to Raman Spectroscopy: Introduction and Basic Principles.
8. Bumbrah, G. S., & Sharma, R. M. (2016). Raman spectroscopy – Basic principle, instrumentation and selected applications for the characterization of drugs of abuse. Egyptian Journal of Forensic Sciences.
9. Skoog, D. A., Holler, F. J., & Crouch, S. R. (2021). Principles of Instrumental Analysis. United States of America.
10. Pandey DK, Kagdada HL, Sanchora P, Singh DK. Overview of Raman spectroscopy: Fundamental to applications. Modern Techniques of Spectroscopy: Basics, Instrumentation, and Applications. 2021:145-84.
11. Uiterl, L. G. (1956). Dielectric Properties of and Conductivity in Ferrite.
12. Liu, S. and Wang, Y., 2010. Application of AFM in microbiology: a review. Scanning, 32(2), pp.61-73.
13. <https://www.nist.gov/image/afmschematic>.

Chapter 5 – RESULTS AND DISCUSSIONS

5.1 X-Ray Diffraction Analysis

The structural properties of Nickel Copper Ferrite nanocomposite were studied using an X-ray powder diffraction (XRD) analysis, conducted on Rigaku Smart Lab Diffractometer using Cu-K α radiation ($\lambda = 1.5418 \text{ \AA}$) as shown in fig 23.



Figure 23: Rigaku Smart-Lab X-ray Diffractometer

The X-ray diffraction patterns and their Rietveld Refinement of the samples are shown in the fig 24. Structural properties of $\text{Ni}_x\text{Cu}_{1-x}\text{Fe}_2\text{O}_4$ ($x = 0.2, 0.4, 0.6, 0.8,$ and 1) ferrites were studied using XRD. The Rietveld refined XRD patterns of powdered samples of nickel copper ferrite indicated the formation of single-phase cubic spinel structure showing well-defined reflections from allowed planes. The lattice constant was found to be increasing with the increase in the concentration of Cu. The variation of the lattice constant with the concentration of nickel is presented in Table 1. All Bragg reflections have been indexed, which confirm the formation of cubic spinel structure in single phase. The strongest reflection are from the (311) plane, which denotes the spinel phase [2]. Peaks indexed to (220), (311), (222), (422), (400), (440) and (511) planes

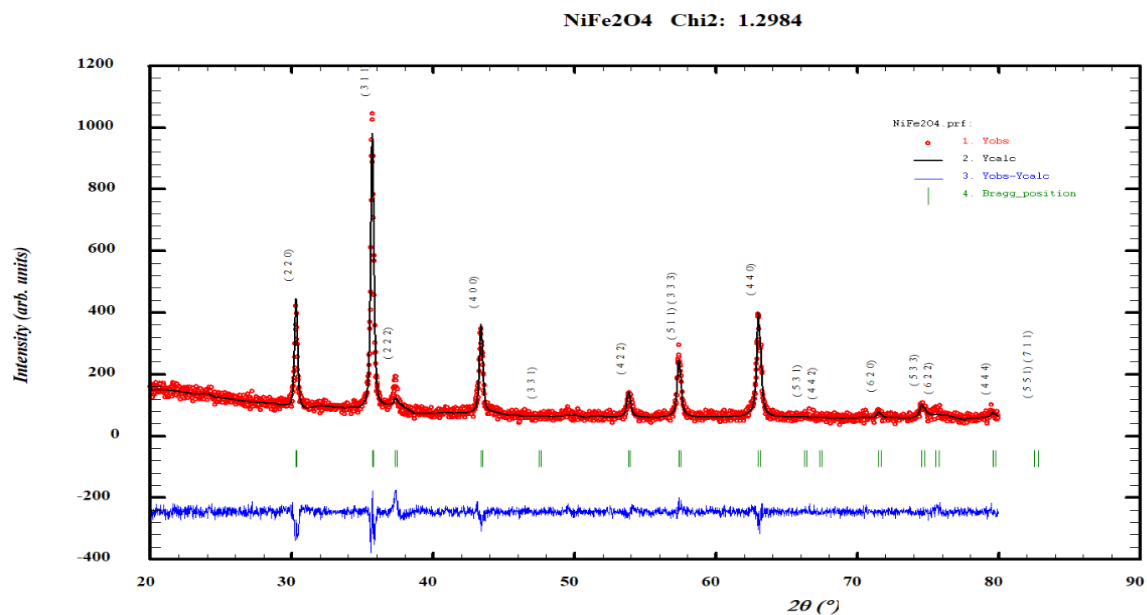
of a cubic unit cell, and all planes are the allowed planes which indicates the formation of cubic spinel structure in single phase [1,9]. The lattice constant is seen to decrease from 8.3626 to 8.3398 Å with increasing Ni content. This increase lattice constant can be because of larger ionic radiuses of Cu^{2+} (0.72 Å) as compared to Ni^{2+} (0.69 Å) [1,10]. The crystallite size was calculated for the all the compositions using the high-intensity 311 peak and using the Scherrer formula .

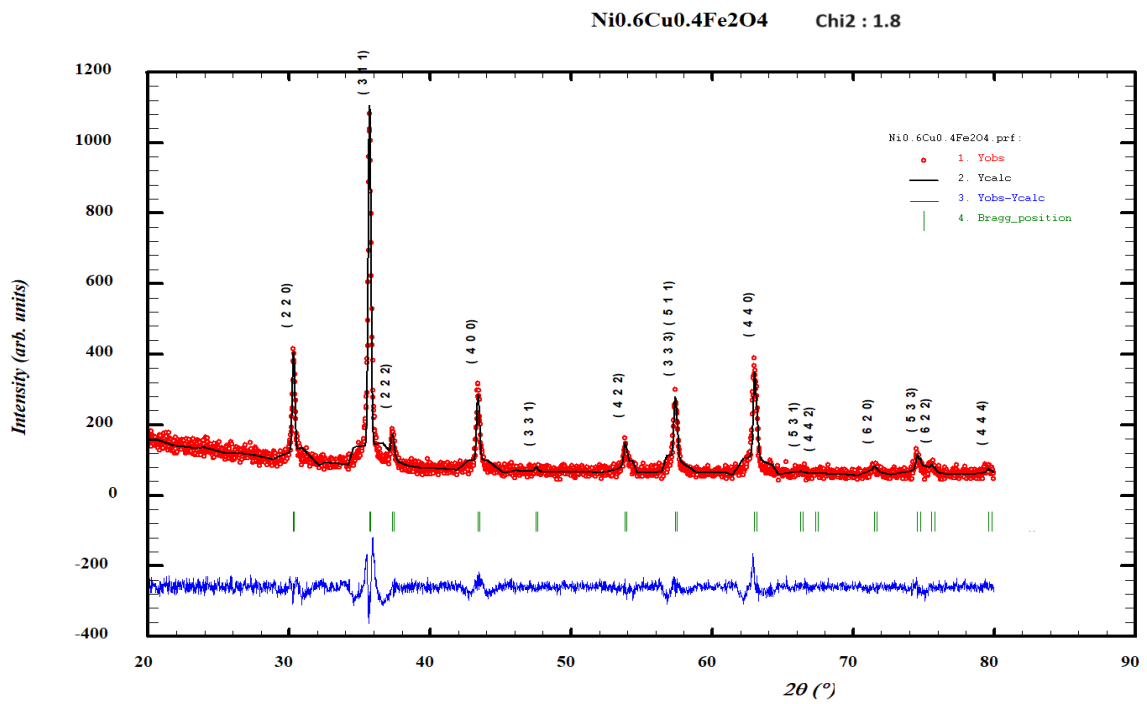
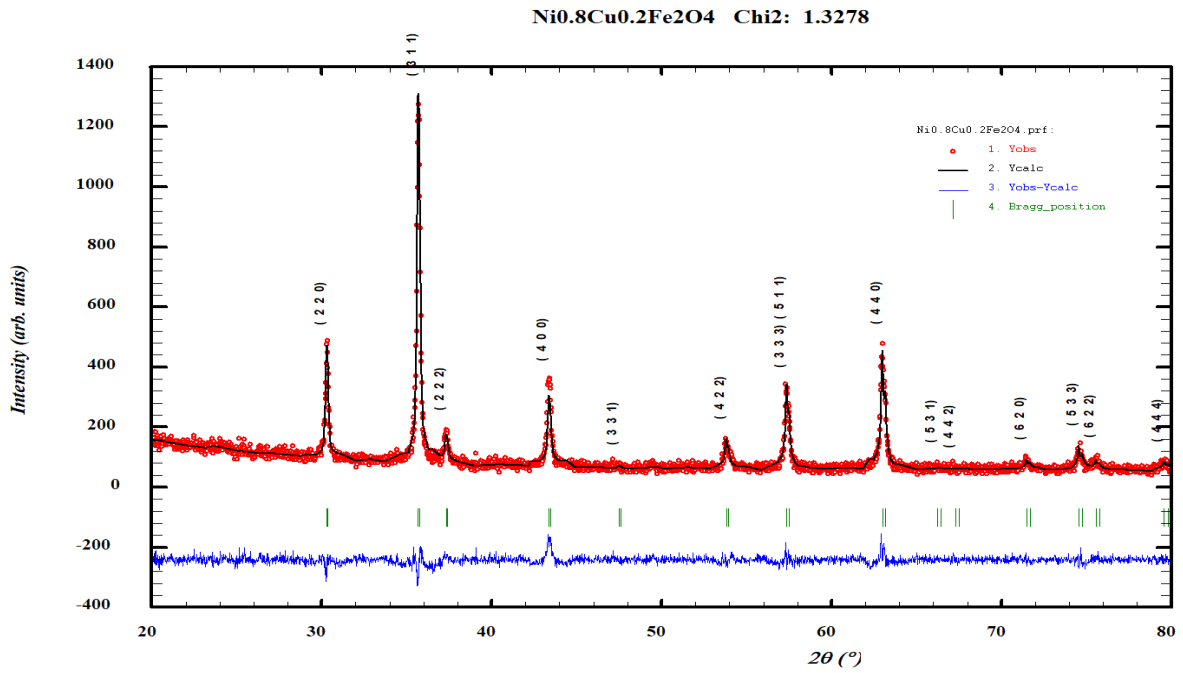
$$D_c = \frac{k \lambda}{\beta \cos\theta}$$

where is D_c crystallite size, β is the full width at half maximum at angle θ , k is a constant and λ is the wavelength of the x-ray source. The crystallite size was found to be between 25-39 nm. The crystallite size increases with the increase in doping of Ni. Strain introduced in powder due to crystal imperfections and distortions is given by,

$$\epsilon = \frac{\beta}{4 \tan\theta}$$

where, ϵ is the strain, β is the full width at half maximum at angle θ . Strain was seen to decrease with increase in concentration of Ni.





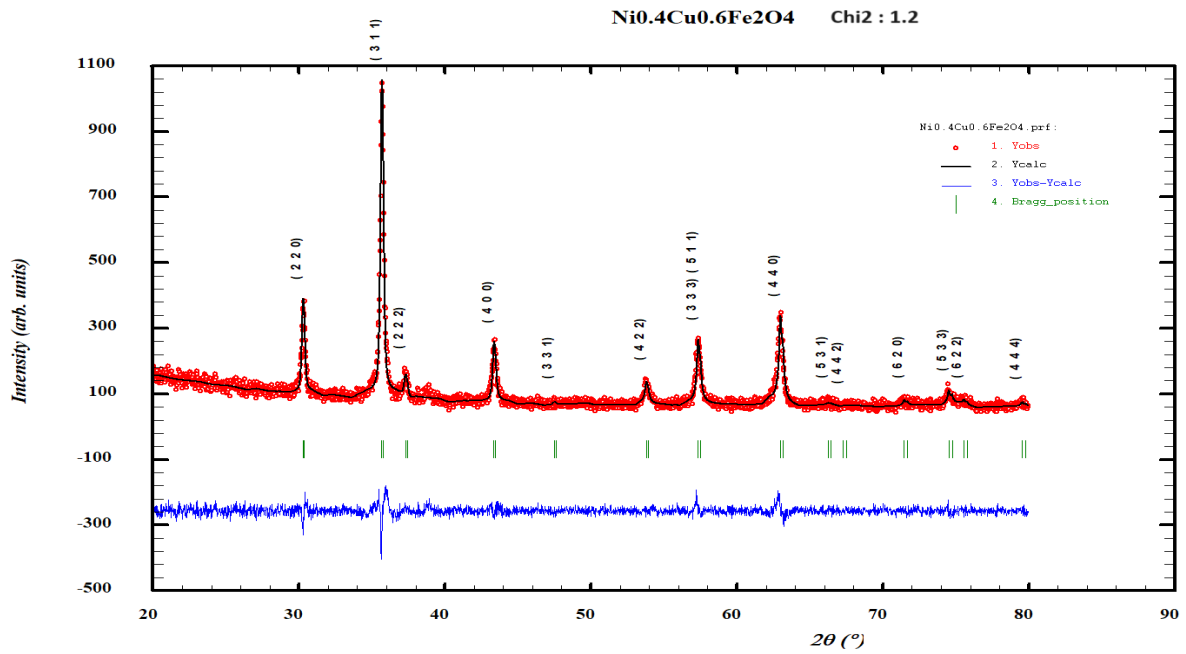
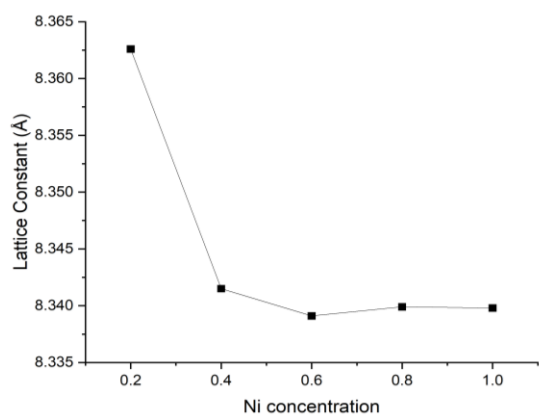


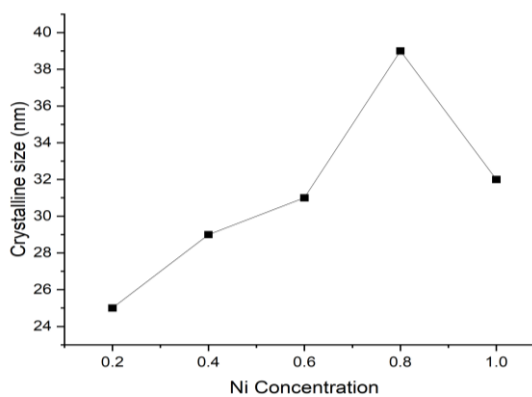
Figure 24 : Reitveld refined XRD patterns of Nickel Copper ferrite nanopowder.

Table 1: variation of lattice constant, crystalline size and lattice strain with increasing Ni concentration.

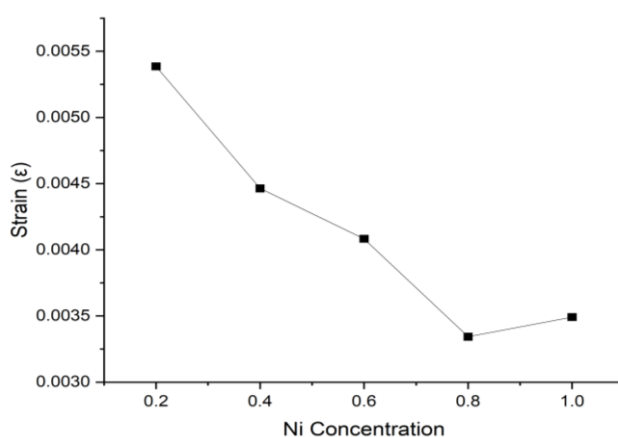
Composition	Lattice constant (Å)	Crystalline size (nm)	Strain (ϵ)
Ni _{0.2} Cu _{0.8} Fe ₂ O ₄	8.3626	25	0.005386
Ni _{0.4} Cu _{0.6} Fe ₂ O ₄	8.3415	29	0.004464
Ni _{0.6} Cu _{0.4} Fe ₂ O ₄	8.3391	31	0.004083
Ni _{0.8} Cu _{0.2} Fe ₂ O ₄	8.3399	39	0.003343
NiFe ₂ O ₄	8.3398	32	0.003492



(a)



(b)



(c)

Figure 25 : (a) Graph of Lattice constant vs Ni concentration (b) Graph of Crystalline size vs Ni concentration (c) Graph of Lattice strain vs Ni concentration

Table 2 : cation distribution in tetrahedral and octahedral sites

	octahedral sites			tetrahedral sites		
	Ni ²⁺	Fe ³⁺	Cu ²⁺	Ni ²⁺	Fe ³⁺	Cu ²⁺
Ni _{0.2} Cu _{0.8} Fe ₂ O ₄	0.24332	1.75063	0.09898	0.03171	0.24997	0.69979
Ni _{0.4} Cu _{0.6} Fe ₂ O ₄	0.26796	1.59096	0.10213	0.02709	0.39872	0.49938
Ni _{0.6} Cu _{0.4} Fe ₂ O ₄	0.40614	1.39608	0.0994	0.01547	0.59885	0.29918
Ni _{0.8} Cu _{0.2} Fe ₂ O ₄	0.7	1.2803	0.01995	0.10031	0.7196	0.1799
NiFe ₂ O ₄	0.09023	0.1855	-	0.01183	0.16387	-

Cationic distribution was calculated by multiplying 7 to occupancies of cations obtained from Rietveld refinement. From cationic distribution (Table 2) in tetrahedral and octahedral sites it can be seen that Ni²⁺ likes to occupy octahedral sites whereas Cu²⁺ wants to occupy tetrahedral sites in the Spinel structure.

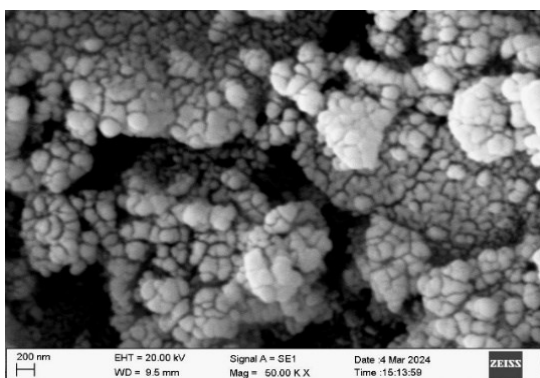
5.2 Scanning Electron Microscope Analysis



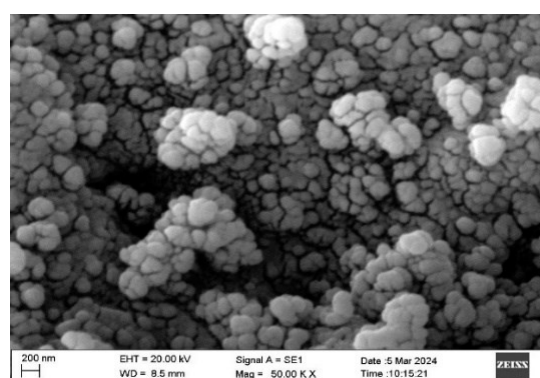
Figure 26: Carl Zeiss Scanning Electron Microscope and Sputter coater setup.

Carl-Zeiss EVO 18 Special Edition Scanning electron microscope was used to study morphology of prepared nanopowder samples. The SEM images were analysed by ImageJ software. Firstly the samples were coated with conductive layer using sputter coater. The images were taken at a resolution of 200 nm. The SEM images for various composition are shown in Fig 26. From the images we see that the particle size of samples lies in nanometer regime and have a spherical shape and nanosized distribution. The particles sharpness is more or less spherical with agglomeration between the particles. The agglomeration is due to high reactivity expected of nanoparticles [1,2]. It can be seen that samples on the surface are highly porous which can be linked to quick exit of high volume of gases produced during combustion. Availability of porous lattice is one of characteristics of producing nanoparticles by combustion method.[1,2]

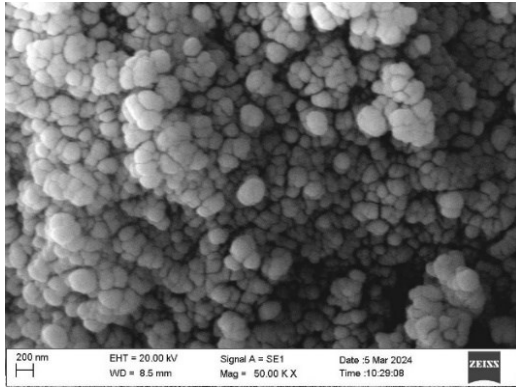
The crystalline size varies from 25 to 39 nm as obtained using Debye -Scherrer formula. The Crystalline size decreases with increase in Cu concentration. It is thus observed that the size of nanoparticles decreases when the concentration of copper is increased because the atomic radius of nickel (0.69 \AA) is less than that of copper (0.73 \AA). From the images it is clear that agglomeration decreases with the increase in Cu concentration.



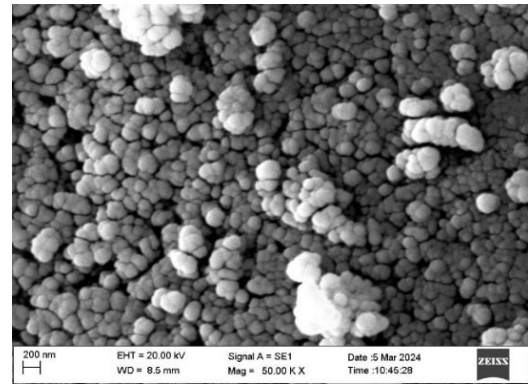
a)



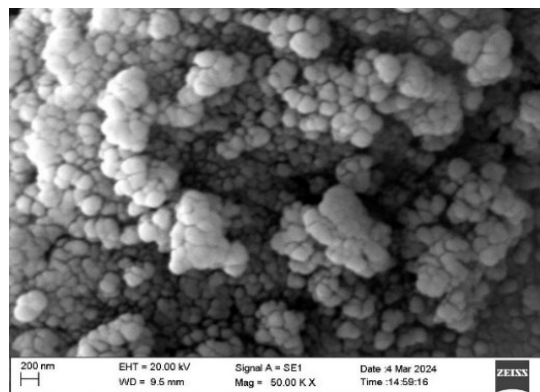
b)



c)



d)



e)

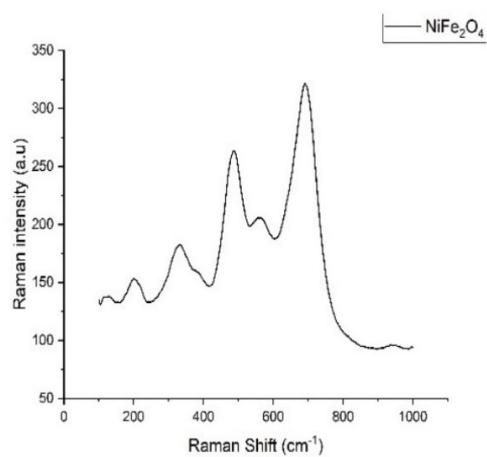
Figure 27: SEM images (200 nm) of a) $Ni_{0.8}Cu_{0.2}Fe_2O_4$ b) $Ni_{0.6}Cu_{0.4}Fe_2O_4$ c) $Ni_{0.4}Cu_{0.6}Fe_2O_4$ d) $Ni_{0.2}Cu_{0.8}Fe_2O_4$ e) $NiFe_2O_4$

5.3 Raman Spectroscopy Analysis

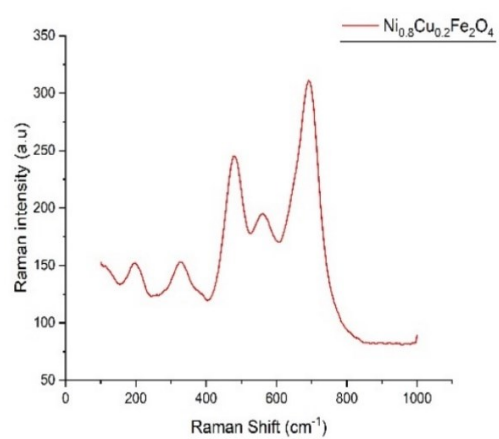


Figure 28 : LabRAM HR Evolution Raman Microscope

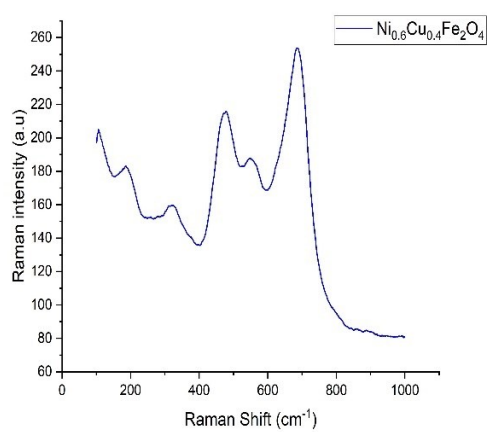
The Raman Spectra of the samples were acquired using the LabRAM HR Evolution Raman Microscope shown in Fig 28. The obtained Raman spectra are shown in the Fig. 27 shows Raman spectra for pure NiFe_2O_4 and copper doped NiFe_2O_4 , prepared by the auto-combustion method. The spinel ferrites have cubic structure belonging to space group $Fd\bar{3}m$. There are five Raman active modes ($A_{1g} + E_g + 3F_{2g}$) which are expected in the spinel structure. The five Raman modes are observed also which are shown in the Fig. 28. In pure Ni ferrite, due to differences in ionic radii of Ni and Fe ions, the Fe/Ni–O bond distance shows a considerable distribution. This means that the local structure in the two cases is different and the Raman spectrum, being a local structure-sensitive tool, detects these changes very effectively. The A_{1g} mode is due to symmetric stretching of oxygen atoms along Fe–O (and Ni–O) bonds in the tetrahedral coordination. E_g is due to the symmetric bending of oxygen with respect to the metal ion and F_{2g} (3) is caused by asymmetric bending of oxygen. F_{2g} (2) is due to asymmetric stretching of Fe (Ni) and O. F_{2g} (2) and F_{2g} (3) correspond to the vibrations of octahedral group. F_{2g} (1) is due to translational movement of the tetrahedron (metal ion at tetrahedral site together with four oxygen atoms). The Raman peaks over the region $620\text{--}720\text{ cm}^{-1}$ shows the alteration in the tetrahedral sites, while those in the $450\text{--}620\text{ cm}^{-1}$ region shows alteration in the octahedral sites.[2] There is a Raman shift in peaks in octahedral sites due to difference in ionic radii of nickel and Copper which results in shorter bond length and Raman shift being bond length sensitive there is shift in the peaks towards higher wavenumbers.



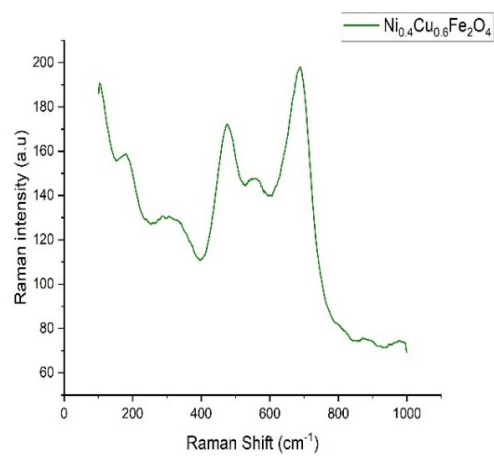
(a)



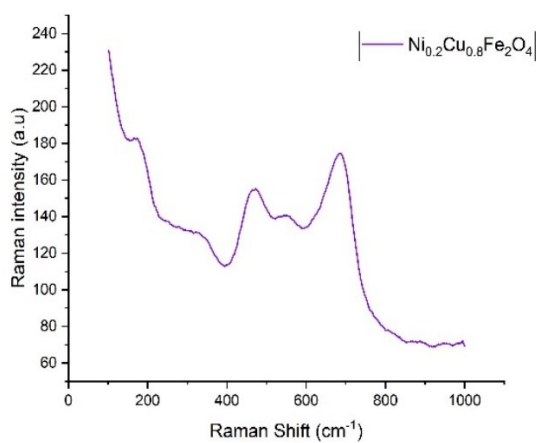
(b)



(c)



(d)



(e)

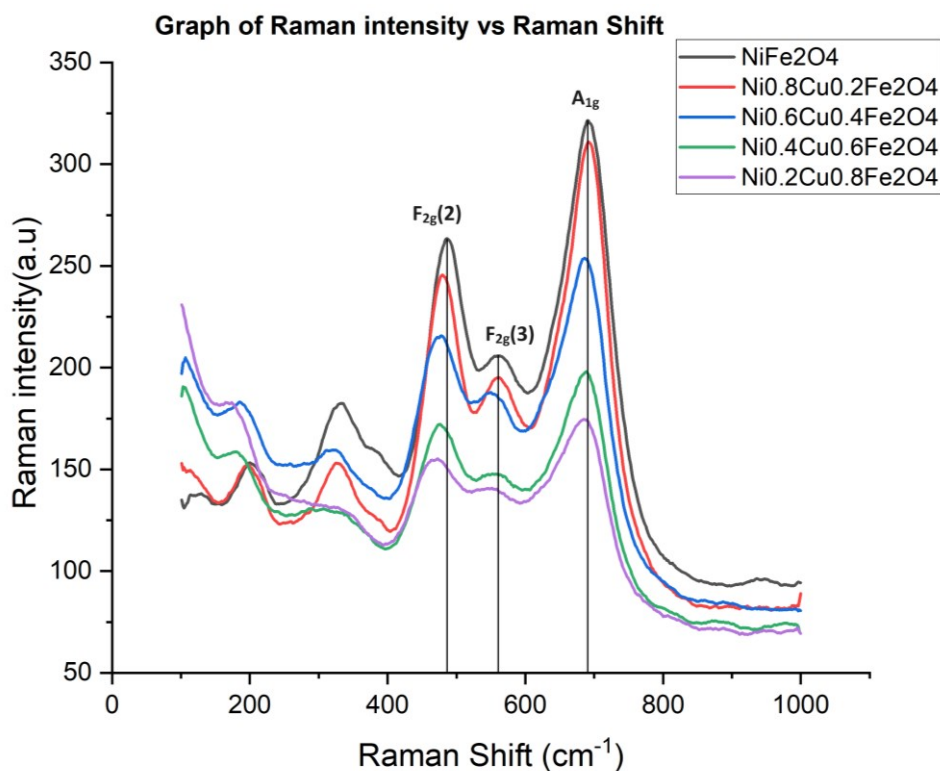


Figure 29: Raman spectra of prepared samples a) NiFe_2O_4 b) $\text{Ni}_{0.8}\text{Cu}_{0.2}\text{Fe}_2\text{O}_4$ c) $\text{Ni}_{0.6}\text{Cu}_{0.4}\text{Fe}_2\text{O}_4$ d) $\text{Ni}_{0.4}\text{Cu}_{0.6}\text{Fe}_2\text{O}_4$ e) $\text{Ni}_{0.2}\text{Cu}_{0.8}\text{Fe}_2\text{O}_4$.

5.4 Electrical Analysis by Network Analyser



Figure 30: Network Analyser Set-up

The electrical analysis was conducted using the LCR meter as shown in the fig 30. In order to perform electrical investigations, depending on the frequency, the disk shaped pellets were prepared using a pelletizer fig 31.



Figure 31: Set up of a pelletizer.

5.4.1 Variation of Dielectric constant with Frequency

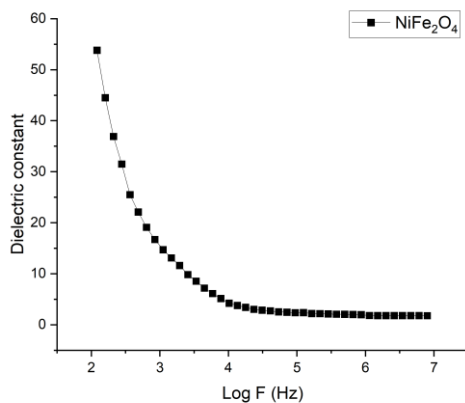
The dielectric constant values of the as prepared samples were plotted as a function of frequency as shown in fig . The relative dielectric constant was calculated using the relation given below

$$\text{Dielectric constant} = \frac{C_p \times t}{A \times \epsilon_0}$$

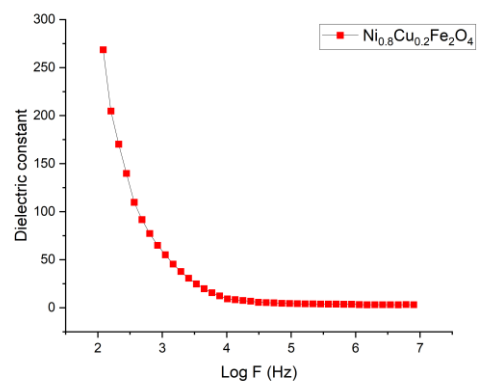
where C_p is parallel capacitance of pellet, t is thickness of pellet, A is the area of pellet, and ϵ_0 is permittivity in free space whose value is 8.85×10^{-12} F/m. From the graph it is clear that the specimen with the composition $\text{Ni}_{0.8}\text{Cu}_{0.2}\text{Fe}_2\text{O}_4$ exhibits the highest value of dielectric constant as it has the maximum divalent iron ion concentration among all the mixed Ni-Cu ferrites [4]. This was because nickel prefers to be at octahedral site hence more of Fe goes to tetrahedral site in Fe^{+2} state. This high value can be explained on the basis of that it has maximum number of ferrous ions whose exchange $\text{Fe}^{2+} \leftrightarrow \text{Fe}^{3+}$ gives rise to maximum dielectric polarization. the variation of the dielectric constant of Ni-Cu ferrites runs parallel to the variation of available ferrous ions on octahedral sites [4]. It is significant to note that $\text{Ni}_{0.2}\text{Cu}_{0.8}\text{Fe}_2\text{O}_4$ which has the

lowest ferrous ion concentration, possesses the lower dielectric constant. is the number of ferrous ions on the octahedral sites that play a predominant role in the processes of conduction as well as dielectric polarization [5]. It can be seen from the figures that the value of dielectric constant decreases continuously with increasing frequency. The decrease of dielectric constant with increase of frequency of the applied electric field can also be explained on the basis of Koop's theory, which assumes that the ferrites are made up of well conducting grains separated by a thin layer of poorly conducting grain boundaries [6]. In the case of $\text{Ni}_{0.8}\text{Cu}_{0.2}\text{Fe}_2\text{O}_4$ the ferrous ion content is higher than that in other mixed Ni-Cu ferrites. As a consequence, it is possible for these ions to be polarized to the maximum possible extent. Further, as the frequency of the externally applied electric field increases gradually, and though the same number of ferrous ions is present in the ferrites material, the dielectric constant decreases. This reduction occurs because beyond a certain frequency of the externally applied electric field the electronic exchange between ferrous and ferric ions i.e. $\text{Fe}^{2+} \leftrightarrow \text{Fe}^{3+}$ can not follow the alternating field [7]. The dielectric materials have conducting grains that are separated by insulating grain boundaries. When the dielectric material is kept in an the ac field, the electrons arrive at the grain boundaries through hopping. They add up at the grain boundaries due to their high resistivity and produce polarization. This type of polarization is called as space charge polarization [8]. The charge carriers take some time to align their axes along with the external applied ac field. When the frequency of an alternating field increases only some small number of charge carriers can reach the grain boundaries and hence charges do not line up with the external applied ac field, as a result of which the polarization lags behind the applied field. The decrease of charge carriers at the grain boundaries reduces the polarization, and thus, the dielectric constant is reduced [8]. The

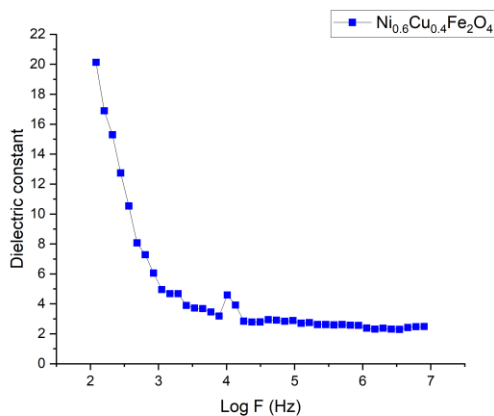
polarization phenomenon in spinel ferrites is exactly similar to the conduction process [9]. The transfer of electron between the ferrous and ferric ions enhances the local displacement of the charge carriers along the direction of external applied ac field that is accountable for the polarization. The exchange of electron between Fe^{2+} and Fe^{3+} do not follow the ac field after a certain frequency so the dielectric constant behaves independent of frequency.



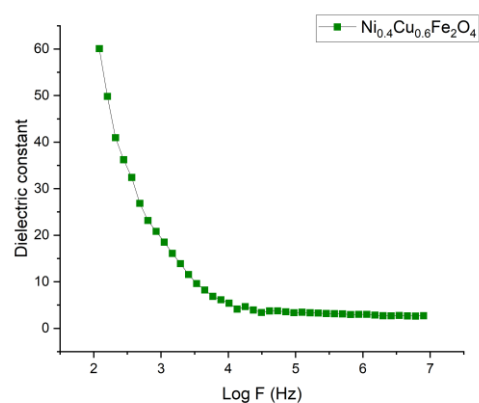
(a)



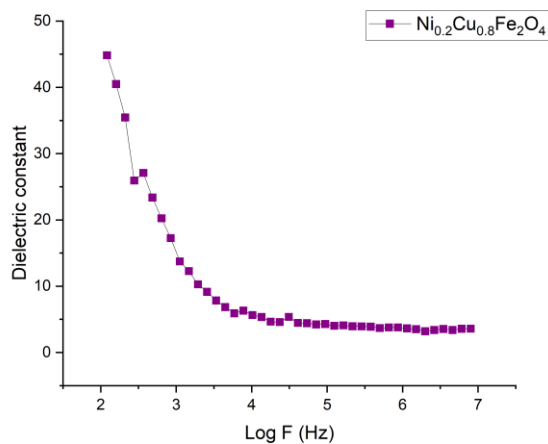
(b)



(c)



(d)



(e)

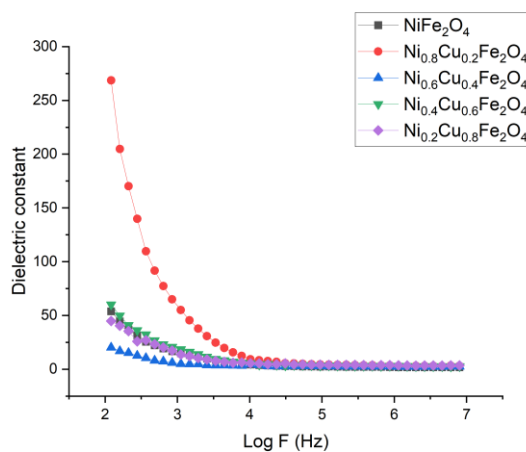


Figure 32: Plot of Dielectric constant vs Log F(Hz) a) NiFe_2O_4 b) $\text{Ni}_{0.8}\text{Cu}_{0.2}\text{Fe}_2\text{O}_4$ c) $\text{Ni}_{0.6}\text{Cu}_{0.4}\text{Fe}_2\text{O}_4$ d) $\text{Ni}_{0.4}\text{Cu}_{0.6}\text{Fe}_2\text{O}_4$ e) $\text{Ni}_{0.2}\text{Cu}_{0.8}\text{Fe}_2\text{O}_4$.

REFERENCES

1. Mahalakshmi S, Srinivasa Manja K, Nithiyantham S. Structural and morphological studies of copper-doped nickel ferrite. *Journal of Superconductivity and Novel Magnetism*. 2015 Oct;28:3093-8.
2. Lassoued A, Lassoued MS, Karolak F, García-Granda S, Dkhil B, Ammar S, Gadri A. Synthesis, structural, optical, morphological and magnetic characterization of copper substituted nickel ferrite ($\text{Cu}_x\text{Ni}_{1-x}\text{Fe}_2\text{O}_4$) through co-precipitation method. *Journal of Materials Science: Materials in Electronics*. 2017 Dec;28:18480-8.
3. Babaei F, Ghasemi A. Structural, optical and magnetic properties of nickel–copper ferrite $\text{Ni}_x\text{Cu}_{1-x}\text{Fe}_2\text{O}_4$. *Optical and Quantum Electronics*. 2022 Nov;54(11):697.
4. L. I. Rabinkin and Z. I. Novikova *Ferrites Minsk*, (1960) p.146 (In Russian).
5. Q. Chen, P. Du, W. Huang, L. Jin, W. Weng and G. Han *Appl. Phys. Lett.* 90 (2007) 132907.
6. Kumar GR, Kumar KV, Venudhar YC. Electrical conductivity and dielectric properties of copper doped nickel ferrites prepared by double sintering method. *International Journal of Modern Engineering Research*. 2012;2(2):177-85.
7. A. Muhammad and M. Asghari, "Structural, electrical and magnetic properties of $\text{Cu}_{1-x}\text{Zn}_x\text{Fe}_2\text{O}_4$ ferrites ($0 \leq x \leq 1$)," *J. Alloys Compounds*, vol. 460, pp. 54–59, 2009.
8. M. A. Ahmed and N. Okasha, "Role of Cu^{+2} concentration on the structural and transport properties of Cr-Zn ferrites," *J. Magn. Magn. Mater.*, vol. 321, no. 20, pp. 3436–3441, 2009.

9. Mazen, S.A., Mansour, S.F., Zaki, H.M.: published on line 15 June 2003. Some physical and magnetic properties of Mg-Zn ferrite. *Cryst. Res. Technol.* 38(6), 471–478 (2003).

Chapter 6 - CONCLUSIONS

Nickel Copper ferrite with composition $\text{Ni}_x\text{Cu}_{1-x}\text{Fe}_2\text{O}_4$ with $x = 0.2, 0.4, 0.6, 0.8,$ and 1 were synthesised using Auto-combustion method. From XRD pattern indicated formation of single-phase cubic spinel structure having space group $Fd\bar{3}m$ showing well-defined Bragg peaks indexed to (220), (311), (222), (422), (400), (440) and (511) planes of a cubic unit cell, and all planes are the allowed planes. The lattice constant was found to be increasing with the increase in the concentration of Cu because of larger ionic radii of copper as compared to that of Ni. The crystalline size was seen to vary from 25-39 nm. SEM images showed agglomeration of particles having spherical shape and also samples were seen to exhibit surface which is highly porous which can be linked to quick exit of high volume of gases produced during combustion.

The highly porous nature of the samples indicates the presence of more active sites which can be linked to increased gas sensing properties. The electrical properties analysis showed that dielectric constant is high for lower frequencies and decreases with increasing frequency. $\text{Ni}_{0.8}\text{Cu}_{0.2}\text{Fe}_2\text{O}_4$ exhibited the highest value of dielectric constant as it has highest ferrous ion content compared to other samples this was because nickel prefers to be at octahedral site hence more of Fe goes to tetrahedral site in Fe^{+2} state. Raman spectroscopy plot showed the Raman peaks over the region $620\text{--}720\text{ cm}^{-1}$ shows alteration in the tetrahedral in ferrites, while those in the $450\text{--}620\text{ cm}^{-1}$ show alteration in the octahedral. Nickel Copper ferrite nanoparticles can have applications in electronic devices like gas sensors. For enhancing the applicative properties of nickel copper ferrite nanoparticles further studies are required.

